Eur. Phys. J. D **42**, 15–34 (2007)
DOI: 10.1140/epjd/e2007-00002-4

THE EUROPEAN PHYSICAL JOURNAL D

Experimental transition probabilities and improved level energies in Yb III*

K.J. Öberg[1,a] and H. Lundberg[2]

[1] Atomic Astrophysics, Lund Observatory, Box 43, 221 00 Lund, Sweden
[2] Department of Physics, Lund University, Box 118, 221 00 Lund, Sweden

Received 15 October 2006 / Received in final form 13 November 2006
Published online 12 January 2007 –

Abstract. Radiative lifetimes of nine out of the twelve $4f^{13}6p$ levels in Yb III have been measured, seven of these for the first time. A Penning discharge lamp is introduced as a continuous plasma source, in which the lifetimes are determined with the time-resolved laser-induced fluorescence technique by pumping from metastable $5d$ and $6s$ levels. Spectra of the same source are recorded with a Fourier-transform spectrometer, which are used to derive branching fractions of the $6p$ and $7s$ levels. Combined with the lifetimes, the branching fractions are used to determine 81 experimental transition probabilities. Wavelengths of 142 Yb III transitions are measured and the uncertainties of corresponding Ritz wavenumbers are improved by an order of magnitude from the prior values. The energy of the $5d\,(5/2{,}5/2)^{\circ}_{0}$ level has been shifted 144.20 cm^{-1} to the higher value 45421.045 cm^{-1}. Much emphasis is put on data treatment and error analysis.

PACS. 32.70.Cs Oscillator strengths, lifetimes, transition moments – 32.30.-r Atomic spectra – 52.80.Yr Discharges for spectral sources (including inductively coupled plasma) – 39.30.+w Spectroscopic techniques

1 Introduction

One of the standard methods for determining radiative lifetimes is by the time-resolved Laser-Induced Fluorescence (LIF) technique, which requires a plasma source that produces free atoms or ions. A common source in these investigations is a cylindrical single-sided Hollow Cathode (HC), from which the atoms and ions are emitted through a small hole in the closed end [1]. The small hole is open to a cell where the plasma beam is probed by LIF. To minimize the effect of collisional deexcitation on the measured lifetimes, the pressure in the cell is lower than in the HC. Strong LIF signals can be achieved by pumping either from the ground state, or from metastable levels. The upper limit to the level energies of the latter is typically 30 000 cm^{-1} for neutral elements and 10 000 cm^{-1} for singly ionized. In most investigations, the HC is pulsed to produce higher densities of both atoms and ions in the plasma beam; and to increase the population of the metastable levels. Another common method to produce free atoms and ions is by laser-ablation of a solid target [2]. In order to minimize collisional deexcitation the ablation target is placed inside a high-vacuum cell, where the lifetimes are measured in the expanding plasma by the LIF technique. Lifetimes in neutral to doubly ionized elements have been measured in ablation plasmas. Also in this plasma the metastable levels are populated. The upper limit to the energy of these levels, from which the plasma can be probed by LIF, is typically 20 000 cm^{-1} for singly ionized elements.

In this work, the Penning Discharge (PD) lamp is introduced as a plasma source for lifetime measurements by the LIF technique. In the continuous discharge of this lamp it is possible to measure lifetimes by pumping from metastable $5d$ and $6s$ levels in Yb III, of which the highest employed in this work has an energy of 51 582 cm^{-1}. Considering it is a doubly-ionized metal, this is high up in the level system compared with earlier investigations using other plasma sources. Radiative lifetimes of nine $4f^{13}6p$ levels in Yb III are measured. Two of these levels have previously been investigated in an ablation plasma by two-photon excitation from the $4f^{14}\,{}^1\mathrm{S}_0$ ground state [3]. However, this technique restricts the J-values of the $6p$ levels to a maximum value of two, since in each excitation step the J-value of the upper pump level cannot differ more than one from the lower.

Doubly-ionized ytterbium is suitable for an investigation of the PD-source for the purpose of lifetime measurements by the LIF technique. Up to a level energy of 53 736 cm^{-1} it has 21 metastable levels, but only three levels with allowed transitions to the ground state. Resolved spectra of the PD-plasma, recorded with a Fourier-Transform Spectrometer (FTS), are analyzed to determine

* Supplementary files concerning Ritz wavenumbers and the associated uncertainties are only available in electronic form at `http://www.eurphysj.org`

[a] e-mail: `kasper@astro.lu.se`

some of the plasma parameters that can influence the lifetime measurements. Parts of this analysis are made possible by the fact that most of the strong transitions in Yb III can be covered by one FTS spectrum.

By combining the measured lifetimes and branching ratios, which are determined from the FTS spectra, 81 experimental transition probabilities are produced. These are in good agreement with the semi-empirical transition probabilities in [3], which indicates that there are no large systematic errors involved in the lifetime measurements. A complete set of lifetimes of the $6p$ and $7s$ levels in Yb III is created by adding some of the semi-empirical atomic data in [3] to this investigation.

In the present work, the PD-source is used for the first time in a spectroscopic study of a rare-earth element. The line intensities of Yb III non-resonance transitions are more than an order of magnitude stronger than in a direct-current HC-source. Combined with the fact that the PD-spectra can be recorded with a FTS, since the discharge is continuous, an improvement of almost all known Yb III level energies is possible. Most of the work regarding level energies of Yb III have been compiled in [4]. Three of the levels in the upper part of the system have been discarded later in [3], where also another 11 level energies were established. In the present work, wavelengths of Yb III transitions between 1900 and 5000 Å are measured. Corresponding wavenumbers are fitted to the level system, thereby improving the accuracy of the level energies by about an order of magnitude from the prior values.

2 The Penning discharge lamp

The design of the Penning discharge lamp used in this work is described in detail in [5] and its use as a spectroscopic light source has been thoroughly investigated in [6]. Two permanent NdFeB magnets, with poles oriented in the same direction, create a homogeneous magnetic field of about 0.1 T between the cathodes, see Figure 1. This field confines the electrons in the discharge plasma radially, forcing them to move in helical trajectories between the cathodes. The electrons leave the discharge region only through repeated collisions with atoms and ions in the plasma. The two opposed cathodes create a symmetric electrical potential, which forces the electrons to oscillate between the cathodes. By this construction of the light source, both the path length and the travel time of an electron in the plasma are increased.

In the experimental setup, two of the ports of the PD-source were connected to T-couplings, of which one was connected to the gas supply and the other to a turbomolecular pump. The PD-source was sealed with UV-grade fused silica windows. The four ports form a cross centered on the discharge region. By this construction, it was possible to send a pump laser pulse through the discharge plasma without hitting the inside of the PD-source. The fluorescence could then be observed in a direction that was perpendicular to that of the laser, without any reflected laser light in the signal.

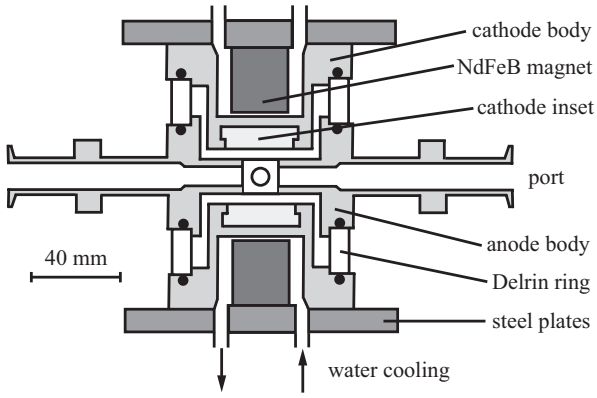

Fig. 1. The Penning discharge lamp used in the investigation. Apart from the steel plates and the four ports, when viewed from above the light source has a circular cross-section. The permanent magnets are aligned so that the magnetic field is homogeneous between the cathodes. The field is confined within the light source by four steel rods connecting the plates. All steel components are ferromagnetic.

The cathode insets were manufactured of commercially 99.5% pure aluminum, which has a low spectral line density and, thereby, decreasing the probability of blends with Yb III lines. Cylinders of 99.9% pure ytterbium were fitted into the center of the cathode insets, with lengths and diameters in the ranges 2.2–5.3 mm and 8.2–9.8 mm, respectively. When recording data, only one of the insets were fitted with an ytterbium cylinder, since it was not possible to sustain a stable discharge when both were fitted. Further, neon was used as buffer gas, since both helium and argon produced an unstable discharge. The working pressures, monitored with a capacitance manometer, were between 0.01 and 0.30 torr. When supplied with a direct current the lamp produces a stable discharge. The discharge currents were in the 0.10–1.20 A range, which gave a typical voltage in the interval 0.8–2 kV between the cathodes and the anode, where the latter was connected to ground. From the amount of aluminum that was sputtered with an ytterbium cylinder fitted in one of the insets, it was evident that the ytterbium contributed significantly to the sputtering process. If a discharge was initialized under normal conditions and the pressure then gradually reduced to zero, it was even possible to sustain a stable pure-metal discharge at currents above 0.8 A. Under normal discharge conditions, the lifetime of an ytterbium cylinder was about 1.5 h, after which most the metal had been deposited onto the anode. The PD-source was dismantled after each run to remove the sputtered metal.

3 LIF measurements

3.1 Experimental setup

Radiative lifetimes were measured using the time-resolved LIF technique with the PD-lamp as an ion source. As details of the laser and detection system can be found elsewhere [7,8], only a brief description is given here. Pulsed

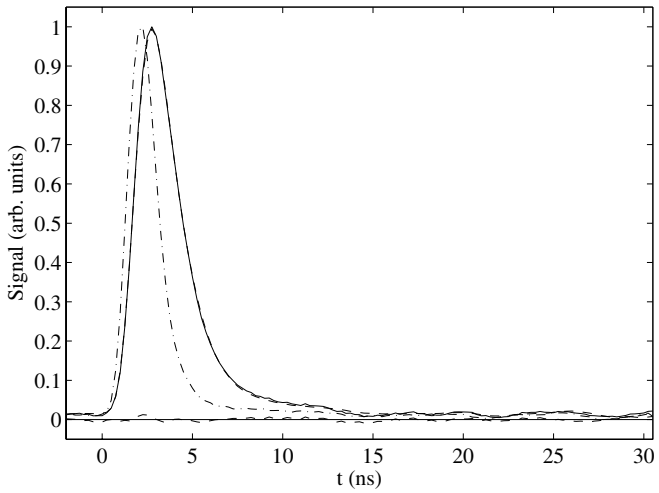

Fig. 2. Time-resolved LIF signal from a PD-plasma of the 37 484.203 cm^{-1} $5d$–$6p$ Yb III transition. The fluorescence signal, which is a sum of 1024 measurements, is shown as a solid line; the fitted convolution and corresponding residual as dashed lines; and the recorded laser signal as a dash-dotted line. Observe that the background signal from other lines in the ytterbium spectrum has been subtracted. The resulting lifetime from this fluorescence signal is 2.36 ns.

tunable radiation for selective excitation in the wavelength region 220–330 nm were produced using a Nd:YAG laser pumped system. A stimulated Brillouin-scattering water cell [7] was used to first compress the Nd:YAG laser pulses in time, which then pumped a dye laser operated with the red dye DCM. The dye laser output was frequency mixed in KDP and BBO crystals and then frequency shifted in a stimulated Raman-scattering hydrogen cell in order to obtain the desired excitation wavelengths. The fluorescence light, released at the decay of the excited ion level, was focused onto the entrance slit of a 1/8 m monochromator (resolution 6.4 nm/mm) equipped with a Hamamatsu R2368 photomultiplier tube with 1.2 ns rise time. Data acquisition was performed with a 1 GHz bandwidth transient digitizer with 2 GS/s sampling rate. The 2 ns pulse width shown in Figure 2 is due to the limited resolution in the detection system, which depends primarily on the rise time of the PM-tube and the dispersion in the signal cable. The true width of the laser pulse is about 1 ns.

3.2 Data analysis

The PD-source was operated continuously during a lifetime measurement, which gave a strong constant background signal from all spectral lines within the bandwidth of the monochromator. Due to this, photon noise dominated over all other noise sources and the strongest fluorescence channel did not always give the best S/N. It can be shown that the observed fluorescence signal on top of the background, see Figure 2, can be expressed as a convolution of the recorded excitation laser pulse and the pure exponential function of the radiative decay [8]. The experimental lifetimes are then derived by a least-squares fit to the fluorescence signals. This method is used when a lifetime is of the same order of magnitude as the width of the laser pulse. The routine used in this work is described in detail in [9].

For the deconvolution method to work, no stray light from the laser pulse can be present in the fluorescence signal. This presented no problem for the non-resonance transitions, since the laser pulses could be led through the PD-source without hitting the inside of the light source and a fluorescence channel different from the pump channel was chosen. To detect the laser signal the pulse was forced to reflect on the inside surface of the PD-source while the monochromator was set to the wavelength of the pump channel. Further, saturation of the upper pump level must be avoided; otherwise, the true time-resolved profile of the pump pulse will differ from the one resulting in the recorded laser signal. This was achieved by lowering the intensity of the pulses, which varied about 60% from the mean, by rotating the KDP crystal until a linear dependence between the pulse and fluorescence signals was observed. For sufficiently long lifetimes, a pure exponential added to a background can be fitted to the part of the decay curve where the laser pulse has ended. Saturation and stray light from the laser have no influence on this method and the same channel for both pumping and fluorescence can be used.

There are two known artifacts present in the fluorescence signals. The first comes from radio signals emitted from the pump-laser system, which results in ringing around the pulse with a slowly changing amplitude and a period of about 12 ns. The same ringing is also present in the recorded laser-pulse signal. Therefore, its effect on the measured lifetimes is small, since these are derived from a fit involving the pulse signal. The second artifact comes from the reflection of the fluorescence signal in the cable between the PM-tube and the transient digitizer, which shows itself as a weak signal with a delay that depends on the length of the cable. The influence of this effect is avoided by simply using a cable length that places the reflection signal outside the part of the fluorescence signal that is investigated.

3.3 Lifetime measurements

Lifetimes for nine $6p$ Yb III levels were measured by pumping from the $5d$ and $6s$ metastable levels, see Figure 3, of which the $5d$ level at 51 582 cm^{-1} was the highest. The remaining three $6p$ levels had no suitable pump channels within the wavelength coverage of the laser system. To increase the S/N, 1024 fluorescence signals were averaged before deriving the lifetime by the deconvolution of the signal profiles described in Section 3.2. Each lifetime was measured at a neon pressure between 0.01 and 0.02 torr and at several different discharge currents ranging from 0.10 to 0.50 A. No dependence on the pressure or the current was found for the measured lifetimes. The signal strengths were the highest at the lowest pressures, but increased rapidly with the current, indicating a strong current dependence for the population density of the $5d$ and

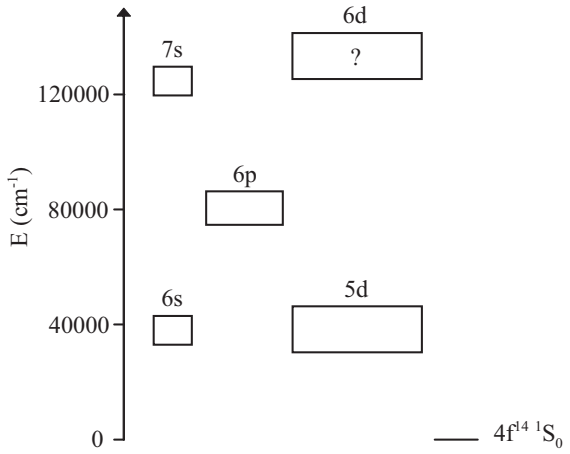

Fig. 3. Simplified energy-level diagram of Yb III, which has the ground configuration [Xe]$4f^{14}$. The $4f^{13}5d$, $6s$, $6p$ and $7s$ configurations have complete sets of observationally determined level energies.

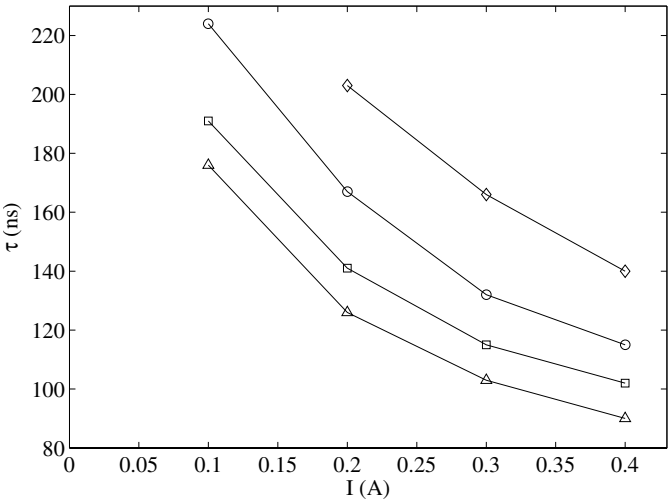

Fig. 4. Lifetime, τ, of the 39721 cm^{-1} Yb III level as a function of the discharge current, I. The four curves correspond to different neon pressures: 0.068 (diamonds), 0.118 (circles), 0.168 (squares), 0.218 (triangles). Clearly, the measured lifetimes depend on both current and pressure. All measurements were performed with the same cathode inset and with about 100 s between them to let the new discharge conditions stabilize.

$6s$ levels. A mean was calculated from the 4–9 best measured lifetimes, chosen by the residuals of the profile fitting. The standard deviation from the mean was typically 5–10%. Even though the number of samples in the mean is too low to yield any significant statistics, a conservative uncertainty of 10% can be assumed for the values of the lifetimes, see further Section 5.1 for another estimate.

From the FTS recordings it was evident that self-absorption never reached more than 1% of the integrated intensity of the $5d$–$6p$ and $6s$–$6p$ line profiles, see Section 4.6. Even though the line intensity increases drastically when a laser excites the upper level, the same percentual drop in the intensity of the fluorescence signal is expected during the decay, since the population density of the lower fluorescence level and the dimensions of the absorbing plasma are approximately the same. Therefore, self-absorption has a negligible impact on the measured lifetimes. It has, however, been assumed that the population of the lower fluorescence level is unchanged during the absorption of the signal, which is practically the case. Saturation was avoided when pumping with the laser, i.e. the time-integrated population density of the upper fluorescence level was always less than half of the initial population density of the lower pump level. The fluorescence photons are radiated isotropically, of which only a fraction of 0.01 fell within the cone of collimated radiation that was observed. Further, the volume of the absorbing plasma was at least an order of magnitude larger than the emitting plasma and the population densities of the lower pump and fluorescence levels were about the same. The total number of ions that could absorb was, therefore, at least 1000 times larger than the total number of collimated photons and only a small change in the number density of the lower fluorescence level was expected.

The lifetimes of the 78 183 and 82 907 cm^{-1} levels have previously been determined by the time-resolved LIF technique to be 1.34(0.10) and 2.53(20) ns, respectively, using a two-photon excitation from the ground state in a laser-ablation plasma [3]. Corresponding lifetimes measured in the present work are 1.48(0.12) and 2.35(0.19) ns, which fall within the combined error bars of the values in [3]. The measured lifetimes of the $6p$ levels are not influenced by collisional deexcitation by electrons, which is shown in Section 5.3.

A lifetime of 230(20) ns for the 39 721 cm^{-1} level has previously also been measured in a laser-ablation plasma, but with a one-photon excitation from the ground state [10]. When this level was investigated in the present work, a strong dependence on the discharge current and the neon pressure was found, see Figure 4. That the apparent lifetime decreases with rising current, i.e. an increase in the electron density, can be explained by a depopulation of the 39 721 cm^{-1} level by electron collisions. Similarly, an increase of the pressure results in a decrease of the apparent lifetime through a more frequent depopulation by gas collisions. However, there are a number of non-linear effects that must be considered. As an example, the discharge plasma is supplied with electrons through the sputtering process. These electrons are accelerated to energies in the 1 keV regime in the sharp cathode fall. Through repeated collisions in the plasma secondary electrons, which can deexcite the investigated levels, are produced by ionization. This process is both current and pressure dependent. Note that the electron temperature is approximately constant with increased current, see Section 5.3.

If the mean free path of the emitted photons is smaller than the dimensions of the plasma, they can be reabsorbed and emitted again. Before the photons are observed, this process can occur several times and in each step the photons change direction isotropically with a time delay that depends on the lifetime of the level and the distance traveled in the plasma. The fluorescence photons are affected

the same way, which results in a longer apparent lifetime. If a homogeneous plasma 10 mm in length is assumed, the self-absorption of 1% gives a mean free path of 1 m for the photons from the $5d$–$6p$ and $6s$–$6p$ transitions, which is too long to have any influence on the measured lifetimes. In contrast to these transitions, the size of the self-absorption of the 39 721 cm^{-1} resonance transitions cannot be determined from relative line intensities, since this is the only downward transition from the upper level. It can, however, be shown indirectly if it is assumed that the metastable $5d$ and $6s$ levels are in thermal equilibrium with the ground state, which is reasonable since the electron velocities are Maxwell distributed and the inverse of the collisional rate is much smaller than the lifetimes involved, see further Section 5.3. With an electron temperature of 14 000 K the $5d$ and $6s$ levels then have a population that is typically a factor 0.01 smaller than for the ground state. The 39 721 cm^{-1} resonance transition has an A-value that is about 100 times smaller than those of the strongest $5d$–$6p$ and $6s$–$6p$ transitions. Combined with the population distribution, this shows that the relative self-absorption of the resonance transition should be of the same order of magnitude as that of the $5d$–$6p$ and $6s$–$6p$ transitions, which never reaches more than 1%. Even if this estimate is too small by a factor of 10, the mean free path of resonance photons is 10 times longer than the diameter of the plasma.

Assuming that self-absorption has a negligible influence on the apparent lifetimes at low currents, it is evident from the slopes of the curves in Figure 4 that the radiative lifetime must be longer than 230 ns that is stated in [10]. Other measurements were performed at lower pressures about 0.01 torr and a current of 0.10 A, resulting in apparent lifetimes between 250 and 270 ns. The PD-source was, however, not stable under these conditions and no sequence of data as the one shown in Figure 4 could be recorded. The difference between the result in the present work and that in [10] is further discussed in Section 6.

4 FTS measurements

4.1 Experimental setup

For the measurement of absolute wavenumbers and branching fractions, spectra were recorded with a Chelsea Instruments FT500 Fourier-transform spectrometer [11]. This instrument has a spectral range of 1900–7000 Å, which covers all strong $5d$–$6p$ and $6s$–$6p$ transitions of Yb III. In the regions 2500–5000 Å and 1900–3500 Å the interferograms were detected with Hamamatsu R955 and R166 PM-tubes, respectively. To enable accurate intensity calibrations, a Schott colored optical glass filter BG24 was placed in front of the R955 PM-tubes in order to avoid light outside the observed alias to be folded into the spectrum. This is not a problem when using the R166 PM-tube, since it has a sensitivity that matches the spectral region 1900–3500 Å.

The PD-source was mounted on an axis that was perpendicular to the optical axis of the FTS. A planar mirror that could be rotated 90° was used to direct the light onto the aperture of the instrument. To enable intensity calibration, a Cathodeon V03 deuterium lamp was mounted on the same axis as the PD-source, but on the opposite side of the mirror. A quartz lens with a focal length of 250 mm, placed between the mirror and the instrument, was used to collimate the light from the two sources. As the discharge region of the deuterium lamp has a diameter of 1 mm and the aperture of the FTS was set to 1.5 mm, the positioning of the lamp and the lens was adjusted so that the light covered the whole aperture. The much larger plasma of the PD-source was simply imaged onto the aperture. The setup was carefully aligned with a laser that backtracked the optical path of the FTS. To prevent light reflected by the back window of the PD-source from reaching the aperture, the source was rotated a few degrees from the optical path. Otherwise, the reflection, which is wavelength dependent, can introduce errors in the intensity measurements.

A HC-source, which is described in [12], was also used in the investigation. The cathode inset was manufactured out of spectroscopically pure iron. A foil of 99.9% pure ytterbium was fitted on the inside of the cathode bore, which was 6 mm in diameter. Apart from the 39721 cm^{-1} resonance transition, the Yb III lines from this source were weaker than those from the PD-source recorded at the same discharge current. By comparing the line intensities in the HC and PD-spectra, it was possible to identify which line that belonged to Yb III, see further Section 5.2. The line widths in the HC-spectra are narrower than in the PD-spectra, which made it possible to measure the intensities of the Yb III lines that were blended in the latter. Further, in order to identify lines blended with the Yb III lines that originate from either the buffer gas, or the aluminum of the cathode insets, PD-spectra were recorded without any cylinder of ytterbium fitted in the insets.

4.2 Correction for correlated noise in the FTS spectra

In a FTS spectrum, the noise is dominated by photon noise, which is distributed evenly and results in a global noise level over the whole spectral range. A known problem with the FTS used in the present investigation is that the noise in the spectra is correlated [12]. This can be shown by taking the autocovariance [13] of a part of the spectrum that is free from spectral lines, i.e. a convolution of this part with itself. A typical autocovariance of the noise is shown in Figure 5, where the correlation is evident from the normalized value of 0.44 at lag 1, showing that there is a contribution to the noise of each data point from those neighboring it. The underlying process is assumed to be described by the moving average

$$y_i = a\,\epsilon_i + (1-a)\epsilon_{i+1}, \tag{1}$$

where ϵ, which has the expectation value $E(\epsilon) = 0$, is a random and uncorrelated variable generated through a white noise process. From this it follows that $E(\epsilon_m\,\epsilon_n)$ is only non-zero if $m = n$, where it equals u_ϵ^2, which corresponds to the standard deviation of the true noise. The

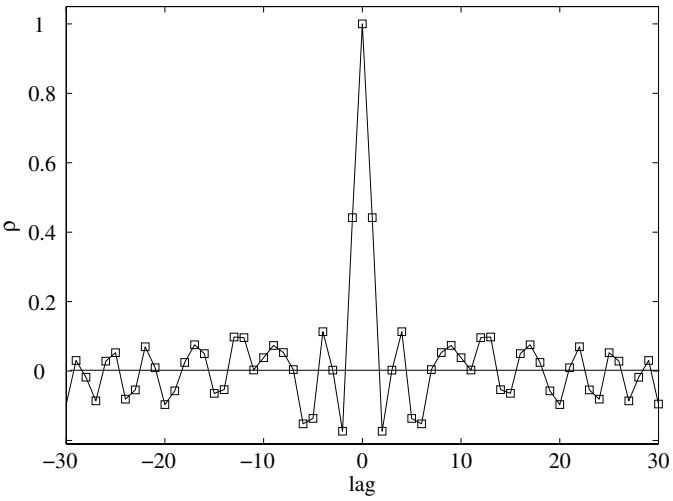

Fig. 5. Autocovariance, ρ, versus lag of a part of a FTS spectrum free from spectral lines. The sequence has been normalized so that the autocovariance is unity at zero lag.

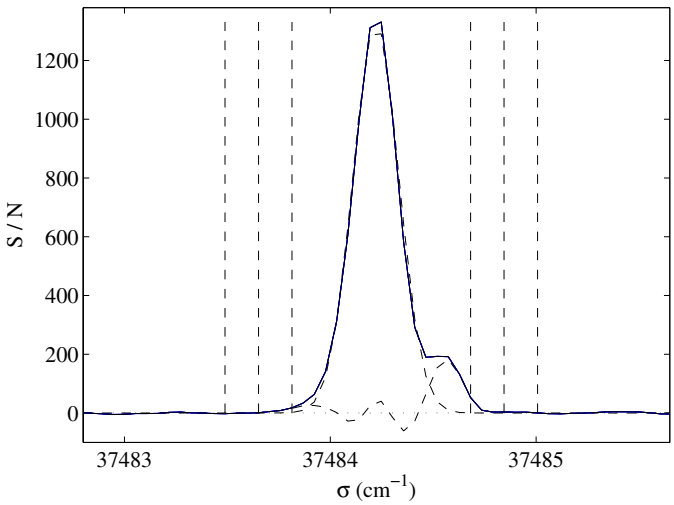

Fig. 6. The $6s$–$6p$ Yb III transition at 37 484 cm^{-1} in a FTS spectrum from the PD-source. The discharge current and neon pressure is of 0.30 A and 0.013 torr, respectively. There is a clear structure in the line profile due to isotope shifts and hfs of the odd isotopes. The fitting of a Gaussian function and corresponding residual are shown as dashed lines. Truncation points for center of gravity measurements are shown as vertical dashed lines, where the outermost correspond to an error over uncertainty ratio ϵ/u of 0.001, the middle ones 0.01 and the innermost 1, see further Section 4.4. The FWHM of the fitted Gaussian is 0.263 cm^{-1}, which corresponds to 4.8 data points at the resolution of the FTS used in the investigation.

variance γ_0 and covariance γ_1 of the observed noise are then given by

$$\gamma_0 = E(y_i\, y_i) = (1 - 2a + 2a^2)\, u_\epsilon^2 \tag{2}$$

and

$$\gamma_1 = E(y_i\, y_{i+1}) = (1 - a)\, a\, u_\epsilon^2. \tag{3}$$

The value of a can be solved from the autocorrelation $\rho_1 = \gamma_1/\gamma_0$, which results in

$$a = \frac{1}{2}\left(1 \pm \sqrt{\frac{1 - 2\rho_1}{1 + 2\rho_1}}\right). \tag{4}$$

The value of u_ϵ is then calculated by simply inserting a into either equation (2) or (3). Note that the square root of the variance γ_0 is the standard deviation u_i of the observed noise. With the assumed moving average (1) the value of u_ϵ^2 has a maximum of twice the value of u_i^2, which is obtained if $|\rho_1| = 0.5$. Regarding the two standard deviations involved, the difference between u_ϵ^2 and u_i^2 can be interpreted as the effective number of independent data points n^* is lower than the actual number n in an interval. As an example, if $u_\epsilon^2 = 2u_i^2$ the ratio n^*/n is asymptotically 1/2 when n goes to infinity. For each spectrum a mean of u_ϵ derived from about 20 evenly spaced intervals, each at least 200 data points long, was used to represent the global noise level. This was typically a factor 1.34 larger than the noise level derived by the ordinary standard deviation of the mean.

4.3 Data analysis

Ytterbium has seven naturally occurring isotopes, of which five have a relative abundance between 12 and 32% [14]. Two of these five are odd isotopes and corresponding line profiles are affected by hyperfine structure (hfs). Further, due to level isotope shifts, the wavenumber of a transition differs between the isotopes. These two effects result in asymmetric line profiles of Yb III, where transitions with a lower $6s$ level have the most prominent structure, see Figure 6. With unresolved components of the spectral lines and without any prior knowledge of the transition isotope shifts or the hfs of the odd isotopes, it is difficult to find an appropriate function that gives the atomic parameter values through a least-squares fit. Instead, the integrated intensity of a spectral line is used as the strength of a transition, while the center of gravity of the profile is used to represent the wavenumber of the transition.

For line analysis of Yb III, FTS spectra of the PD-source were recorded in the region 30 000 to 52 000 cm^{-1} at the discharge currents 0.30, 0.60, 0.90 and 1.02 A. Two ytterbium spectra in the region 22 000 to 44 000 cm^{-1} were also recorded at the currents 0.30 and 0.60 A. In all of these recordings the neon pressure was held constant at 0.013 torr. At a current of 0.30 A the voltage over the PD-source was typically around 1 kV and increased linearly 0.1 kV for each step of 0.1 A.

4.4 Line intensities

As the interferograms were recorded using PM-tubes, the area under a line profile is proportional to the number of emitted photons. Here, the line intensity I is defined as the area of a line profile, which is calculated by summing

the intensity y_i in each data point i over an interval that covers the line profile, i.e.

$$I = \frac{d}{2}(y_1 + y_n) + d\sum_{i=2}^{n-1} y_i, \tag{5}$$

where d is the dispersion of the data points. The area measurement is truncated at the exact position of the end points $i = 1$ and n. Therefore, only half of the intensity of these data points is included in the area. Through error propagation, the corresponding variance of the line intensity is given by

$$u^2(I) = u^2(y)\, d^2 \left(n - \frac{3}{2}\right), \tag{6}$$

where $u(y)$ is the global uncertainty of the intensity in each data point, see Section 4.2.

Clearly, the choice of end points influences the uncertainty of the line intensity measurement, since the uncertainty is proportional to the square root of the number of data points within the integration interval. In order to minimize the uncertainty, the end points must be chosen so that they truncate the line profile where the error caused by the truncation is smaller than the uncertainty. If the line profile can be fitted by a known function, the truncation error ϵ at any point on the profile can be calculated from the integral of the function. The end points are then chosen as the first data points where the ratio of the error over the uncertainty ϵ/u is below a certain limit, see Figure 6. This method has the advantage of being reproducible, which is not the case for the more common procedure for measuring the area under a line profile with undefined structure, where the end points are defined graphically by hand. If the function used in the fitting does not correspond to the underlying function of the wings of the line profile, i.e. the residuals are large and systematic; the truncation method does not work for the purpose of error estimates. It can, however, still be used to provide a reproducible method for defining the end points.

The truncation method presented here was used to measure the line intensities of Yb III. Due to the asymmetries of the line profiles, the fitted Gaussian function resulted in systematic residuals. The transitions with the largest residuals were those with $6s$ level involved, see Figure 6. An apparent error over uncertainty ratio ϵ/u was set to 0.001 for these transitions, while for all other it was set to 0.01. In a few cases one of the end points fell upon the wing of a nearby spectral line and had to be defined by hand.

4.5 Branching fractions

A transition probability is derived experimentally by combining a radiative lifetime and a branching fraction. The latter is defined as the fraction of a level population that is deexcited through a specific radiative transition. In order to derive branching fractions of a level from several spectra, scaling factors for the differences in intensity were needed. A main spectrum was chosen, where most of the line intensity measurements were performed. A normalization factor was calculated for each combination of main and secondary spectra and each level, since the relative population of the levels may differ between the spectra. Only a single line was used when normalizing. The normalization factor r_p is then given by $r_p = I_p/I_p^*$, where I_p and I_p^* are the calibrated line intensities, see Section 4.6, of the same transition in the main and secondary spectrum, respectively. The branching fraction of a transition k is then given by

$$BF_k = \frac{r_k\, I_k}{\sum_p \left(r_p \sum_{q\in Q_p} I_q\right)}, \tag{7}$$

where I_k and I_q are the calibrated line intensities, which only need to be relative. Here, r_k and $r_p = 1$ when the corresponding line intensity is measured in the main spectrum, which includes all normalization lines. In the denominator p is summed over all normalization factors and Q_p is the set of lines normalized by the factor r_p. Observe that the same normalization line can be used for several spectra. Through error propagation, the relative variance of BF_k is then given by

$$\begin{aligned}\frac{u^2(BF_k)}{BF_k^2} = {} & (1 - 2BK_k)\frac{u^2(I_k)}{I_k^2} \\ & + \sum_r BF_r^2\ \alpha_r^2 \frac{u^2(I_r)}{I_r^2} \\ & + \sum_s \left(\sum_{t\in T_s} BF_t\right)^2 \frac{u^2(I_s^*)}{I_s^{*2}},\end{aligned} \tag{8}$$

where $u(I)$ is the uncertainty of the calibrated line intensity given by equation (12). All transitions from the investigated level are included in the sum over r. The sum over s includes all normalization lines measured in the secondary spectra and T_s is the set of all branching fractions where the line intensities in the numerator are normalized with the transition s. In the first sum of terms $\alpha_r = 1$ if the transition is not a normalization line, else

$$\alpha_r = 1 + \sum_{u\in U_r} \left(\frac{1}{I_u^*} \sum_{v\in V_u} I_v^*\right), \tag{9}$$

where all line intensities are measured in secondary spectra. Further, V_u is the set of all line intensities that are normalized with I_u^*, which in turn belongs to the set U_r of all line intensities in the secondary spectra of the transition r. Apart from the covariances that are introduced in the normalization, i.e. α_r and the second sum of terms in (8), the equation for the uncertainty of branching fractions is the same as in [15], where the uncertainty of branching fractions has been thoroughly discussed. Note that the normalization method presented here makes it possible to combine spectra from different sources, e.g. from a HC and a PD.

4.6 Intensity calibration

The measured line intensities of the Yb III lines were corrected by the response of the experimental setup, i.e.

$$I_c = \frac{I_o}{R_r\, R_w\, R_c}, \tag{10}$$

where I_o is the observed line intensity of a transition, I_c the corrected intensity, R_r the response of the FTS, R_w a factor that compensates for absorption in the silica window of the PD-source and R_c a factor that corrects for metal-coating of the same window. Observe that all factors in the denominator are wavenumber dependent and that only relative intensities of the Yb III lines are of interest.

To derive the response R_r of the FTS, spectra from a Cathodeon V03 deuterium (D2) lamp were recorded both before and after each recording of an ytterbium spectrum. This lamp has a smooth spectral radiance in the region 1660 to 3580 Å, outside which emission lines are superimposed on the continuum. The spectral radiance of the D2-lamp has been determined at the PTB in Berlin, using the BESSY synchrotron source as the primary radiation standard. The D2 spectra were sampled with the same aperture diameter as the ytterbium spectrum, but at a lower spectral resolution to enable more FTS scans to be added, which increases the S/N. The resolution was, however, sufficient to resolve the emission lines of the D2-lamp between 3600 and 4100 Å. By binning the D2 spectra with the trapezoidal band pass of the monochromator at PTB, it was possible to determine the response of the FTS also for the region with emission lines. The response R_r was calculated as the observed spectral power of the D2-lamp divided by the spectral radiance of the reference data.

A known problem with D2-lamps as transfer standards is that the spectral radiance changes with the age. The D2-lamp used in this work has been employed in other investigation over a period of eight years. In order to determine the change in relative spectral power, branching ratios of $4s$–$4p$ and $4p$–$5s$ transitions in Fe II were derived from HC spectra recorded in the year following the calibration of the D2-lamp, which were compared with the same branching ratios derived from HC spectra recorded after the ytterbium spectra. The comparison was limited by the uncertainty of the measured intensities, which gave an upper limit to an error of 3.5% between 35 000 and 45 000 cm^{-1} (2900 and 2200 Å) for the relative intensities. It has been shown that the absolute spectral radiance of a Cathodeon V04 D2-lamp over a period of twelve years did not change more than 2.5% in the region 1900 to 3400 Å [16], while the relative spectral power changed even less. The only difference between this lamp and the Cathodeon V03 used in the present work is that V04 has a window of Spectrosil, while V03 has a window of MgF_2, which degrades faster.

The imaging of the D2 discharge plasma upon the aperture of the FTS also introduces an error in the observed spectral power. A maximum error of 1.5% between 36 000 and 46 000 cm^{-1} was estimated from a sample of D2 spectra where the position of the lamp was changed after each recording. A relative uncertainty of 4% is given for the reference data obtained at PTB. Roughly, the absolute spectral radiance increases linearly between 25 000 and 50 000 cm^{-1}, from which a linear increase of 1.6% over 10 000 cm^{-1} was estimated for the uncertainty of the relative spectral power. Both the error due to aperture illumination and the uncertainty of the reference data are, however, assumed to be incorporated in the 3.5% error due to the aging of the D2-lamp, since they are coupled to the results of that investigation.

In order to determine the window absorption factor R_w, a spectrum of the D2-lamp was recorded with a clean silica window, identical to those of the PD-source, placed between the lamp and the FTS. This spectrum was divided with another one recorded without a window. The ratio was then fitted with a second-degree polynomial, which was used to calculate the factor R_w at specific wavenumbers. The absorption corresponded to a line-intensity drop of 10% when going from 37 000 to 48 000 cm^{-1}. From the residual of the fit, the maximum relative error of R_w was estimated to be 2%, which was reached after a span of 10 000 cm^{-1}.

As for the response of the FTS, the correction factor R_c for the coating of the PD window varies between the recorded spectra. During the operation of the PD-source, sputtered ytterbium was deposited onto the silica window, which lowered the transmittance. This was a slow process that was noticed first after all the data sampling had been done, i.e. after more than 40 hours of operation. Note that the six spectra used in the investigation took about an hour each to record.

To determine R_c, an additional ytterbium spectrum was recorded with a clean window mounted on the PD-source. Ratios were formed between the intensities I_o of Yb III transitions measured in a spectrum recorded with a coated window and corresponding intensities from the spectrum with a clean window. The strongest transitions were excluded, since they were affected by self-absorption. The decrease in the ratios as a function of wavenumber followed a linear dependence, which corresponded to a drop in the measured line intensities of about 25% between 36 000 and 44 000 cm^{-1}. The factor R_c were determined by fitting a linear function to the ratios and from the residual of the fit a relative error of 2% was estimated for the correction. Several of the spectra were recorded close in time and corresponding values of R_c had a small spread. It was, therefore, assumed that the amount of coated material was constant during each recording. Further, a large change in the relative intensities when recording a spectrum would have been obvious when transforming the interferograms.

Only relative intensities are of interest when deriving the branching fractions. Therefore, errors from the corrections described above depend on the separation in wavenumber between the two lines that are compared. A linear dependence was assumed and since the errors are systematic, they were simply added together. For each group of transitions sharing the same upper level, the errors were derived relative to the wavenumber, σ_1, of the

strongest transition, i.e.

$$\epsilon = \frac{|\sigma - \sigma_1|}{10\,000}\,\beta_1 + \beta_2, \qquad (11)$$

where $\beta_1 = 0.075$ and $\beta_2 = 0$ if $|\sigma - \sigma_1| \leq 10\,000$ cm^{-1}. Since the error introduced in the window absorption correction R_w reached a maximum after 10 000 cm^{-1}, $\beta_1 = 0.055$ and $\beta_2 = 0.02$ if $|\sigma - \sigma_1| > 10\,000$ cm^{-1}. Note that for a line in a secondary spectrum, the value of ϵ was derived from the wavenumber difference between this line and the normalizing line, which, in the secondary spectrum only, has an ϵ of zero.

To determine the relative uncertainty of the calibrated intensity I_c the error ϵ is treated as a relative standard error, even though it is systematic, and is added in quadrature to the statistical uncertainties, i.e.

$$\frac{u^2(I_c)}{I_c^2} = \frac{u^2(I_o)}{I_o^2} + \frac{u^2(I_{D2})}{I_{D2}^2} + \beta_{SA}^2 + \epsilon^2. \qquad (12)$$

Here, $u^2(I_o)$ is the variance of the measured line intensity given by equation (6). The variance $u^2(I_{D2})$ of the binned spectral power I_{D2} of the D2-spectrum was derived from the standard deviation from a second degree polynomial fitted to a part of the D2-spectrum. The term β_{SA} was set to 0.01 to include the error due to self-absorption, which defines a lowest possible relative uncertainty of 1%. This was estimated from the branching ratios formed by the strongest and second strongest transitions from each $6p$ level. When comparing the ratios from spectra recorded at a discharge current of 0.30 and 0.60 A, the differences never exceeded 1.0%. In a HC-source the self-absorption increases linearly with the current under moderate discharge conditions [15]. If the same dependence is assumed for the PD-source, the self-absorption at 0.30 A should have a maximum of 1% of the line intensity.

4.7 Center of gravity

The center of gravity of a line profile, measured over an interval with the end points $i = 1$ and n, is given by

$$\sigma_c = \frac{d}{6I}\sum_{i=1}^{n-1}(2y_i\sigma_i + y_i\sigma_{i+1} + y_{i+1}\sigma_i + 2y_{i+1}\sigma_{i+1}), \quad (13)$$

where I the line intensity or area of the profile over the same interval, d is the dispersion of the data points, y_i and σ_i the intensity and wavenumber at the ith data point. The corresponding variance of σ_c is given by

$$u^2(\sigma_c) = \left(\frac{d\,u(y)}{I}\right)^2 \left\{ \left(\frac{1}{6}(2\sigma_1 + \sigma_2) - \frac{1}{2}\sigma_c\right)^2 + \left(\frac{1}{6}(2\sigma_n + \sigma_{n-1}) - \frac{1}{2}\sigma_c\right)^2 + \sum_{i=2}^{n-2}\left(\frac{1}{6}(\sigma_{i-1} + 4\,\sigma_i + \sigma_{i+1}) - \frac{1}{2}\sigma_c\right)^2 \right\}, \qquad (14)$$

where the global noise is represented by $u(y)$. Clearly, the uncertainty $u(\sigma_c)$ is proportional to the dispersion d but inversely proportional to the area I of the profile. Also, the contribution from each data point is weighted with the distance from σ_c. To minimize the uncertainty of the measurement, the end points should, therefore, be chosen so that they truncate the line profile without introducing an error that is larger than the uncertainty. The same method to determine the end points as for the area measurements was used here, see Section 4.5, which gives uncertainties of the values of σ_c that are roughly inversely proportional to the S/N of the spectral lines. This is the same dependence as for the uncertainty of line center position that is determined by fitting a Gaussian function [15]. Note that the center of gravity measurement is much more sensitive to truncation errors than line intensity measurements, which is why the error over uncertainty ratios ϵ/u were assigned the small values of 0.01 and 0.001.

For the Yb III transitions observed in this work with no $6s$ level involved, i.e. where an ϵ/u equals 0.01, the proposed truncation method gives an $u(\sigma_c)$ of 0.0033 and 0.0012 cm^{-1} for a S/N of 40 and 180, respectively. If the smaller ratio of 0.001 is used this gives values of $u(\sigma_c)$ that are a factor 1.5 larger. Instead, if a Gaussian function is fitted to the line profile, the uncertainties of the line center positions are 0.0017 and 0.0005 cm^{-1}, respectively, which are smaller but of the same order of magnitude.

4.8 Wavenumber calibration

Ne II $3s$–$3p$ transitions of ^{20}Ne have been suggested as tertiary wavenumber standards [12] and were used to set the wavenumber scales of the ytterbium spectra with the free spectral range 22 000–44 000 cm^{-1}. The same deconvolution of the Ne II isotope structure and method to calibrate the wavenumber scale as described in [12] were used. To set the scale of ytterbium spectra in the range 30 000–52 000 cm^{-1}, 84 Yb II non-resonance transitions in the overlap of the two regions were used as transfer standards. The line profiles of these transitions showed asymmetries similar to those of Yb III and corresponding wavenumbers were measured using the method described in Section 4.7. When calculating the mean of the wavenumber correction α [12] from the Ne II and Yb II transitions the reduced χ^2 was close to unity for all spectra, indicating that the uncertainties involved had been estimated with good accuracy. Through error propagation, the uncertainties of the reference data and the wavenumber measurements were combined to form a total uncertainty of the calibrated wavenumbers of the Yb III transitions.

In high current spectra the strongest Yb III transitions were affected by self-absorption, which affects the measured wavenumbers due to the asymmetry of the line profiles. To minimize this effect, the wavenumbers of the strong transitions were measured in spectra recorded at low discharge currents. It is specified in Table 3 in which spectrum each wavenumber was measured.

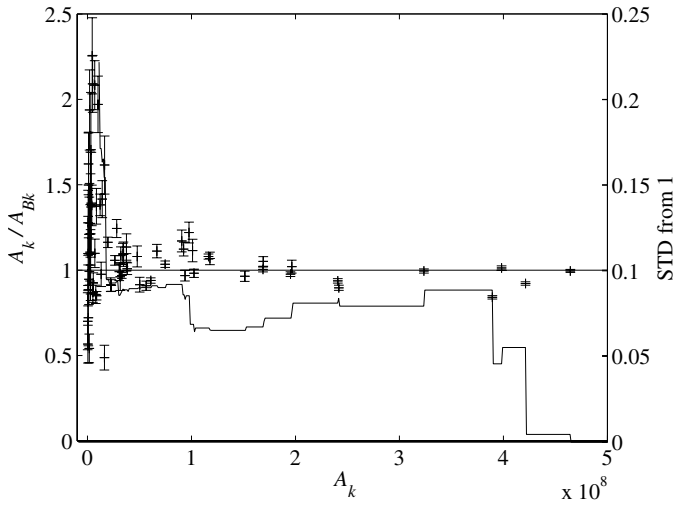

Fig. 7. The ratios between transition probabilities measured in this work, A_k, and those in [3], A_{Bk}, depicted with error-bars that only include the uncertainties of corresponding branching fractions BF_k. The standard deviation (STD) from the expected ratio of one is shown as a graph, which is first calculated for the largest A_k and then by gradually including smaller values.

5 Results

5.1 Branching fractions and transition probabilities

The branching fractions, BF_k, and the associated uncertainties, $u(BF_k)$, for all observed transitions are presented in Table 1. Corresponding transition probabilities were derived using

$$A_k = BF_k/\tau, \tag{15}$$

where τ is the radiative lifetime of the upper level. In Figure 7 it is shown that for the stronger transitions there is a good agreement between the experimental transition probabilities of this work and the semi-empirical values in [3]. Therefore, for levels without measured lifetimes, a value of τ was calculated from the experimental BF_k of the strongest transition and corresponding transition probability in [3]. This lifetime was then used to derive transition probabilities of all transitions from the levels.

None of the levels in Table 1 has a complete set of transitions to lower levels. For each level, all transitions were identified that were not observed but allowed by parity change and J-value selection rules. An upper limit to the line intensities of these transitions was estimated by defining a lowest possible observable S/N of 2, which was multiplied with the typical width of 0.2 cm^{-1} for an Yb III line. These intensities were then calibrated by the same method as the observed transitions, see Section 4.6, and summed together. The sum was inserted in the numerator of equation (7) to form the residual r_1 of the branching fractions, see Table 1. The residual can be interpreted as a percentual systematic error that should be subtracted from all observationally derived branching fractions of a level. By the nature of the derivation, the residuals r_1 are conservative upper estimates. Furthermore, the values of r_1 for all $6p$ levels are less than 0.7 times the lowest uncertainty $u(BF_k)$. The residuals r_1 have, therefore, not been taken into account for the given branching fractions of the $6p$ levels in Table 1.

Residuals r_2 have also been derived from the transition probabilities in [3]. The accuracy of the transition probabilities in [3] is unknown; therefore, these residuals are not compensated for. However, only the 120 247 cm^{-1} and 130 551 cm^{-1} levels have $u(BF_k)$ that are larger than corresponding r_2. For these two levels the residual r_2 can be adopted as the lower limit of $u(BF_k)$, thereby covering the possible error.

In Figure 7 the experimental transition probabilities in this work have been divided by the corresponding semi-empirically calculated values in [3]. Note that only ratios based on transition probabilities derived from experimental lifetimes are used. Clearly, there is a good agreement between the A-values larger than 3×10^7 s^{-1}. The standard deviation $u(R)$ from the expectation value of one, i.e.

$$u(R) = \left[(1/N)\sum(R_k - 1)^2\right]^{1/2}, \tag{16}$$

where R_k belongs to the set of N individual ratios, has a value of about 0.08 for A-values larger than 1×10^8 s^{-1}. Even though there can be systematic errors involved, it is probable that $u(R)$ can be used as an upper limit to the relative uncertainty of the experimental values of A_k. Further, this gives an upper limit of 8% to the relative uncertainties of the measured lifetimes, since this uncertainty is added in quadrature to the relative uncertainty of the branching fractions, of which the lowest ones have a value of about 1%. If there is only a systematic error in either this work or in [3] it is included in the uncertainty estimate. This is also the case if there are systematic errors in both investigations and the influences on the true values diverge.

5.2 Energy levels and Ritz wavenumbers

In order to derive Ritz wavenumbers, σ_{Ritz}, of the transitions in YbIII presented in Table 3, the calibrated wavenumbers were fitted to the level system by the same least-squares method as in [12]. To compensate for underestimated uncertainties or errors, a correction factor k_1 of 1.33 had to be introduced, i.e. all uncertainties u_{obs} derived by equation (14) were multiplied by this value before the fitting. A probable large contribution to the error comes from self-absorption of the strongest $5d$–$6p$ and $6s$–$6p$ transitions, which was minimized by the procedure described in Section 4.8.

The absolute level energies are strongly influenced by the 39 721 cm^{-1} resonance transition, due to the high S/N of this line compared with the two other resonance transitions. Self-absorption in the 39 721 cm^{-1} line can, therefore, cause a systematic shift in all absolute level energies. It is shown in Section 3.3 that the self-absorption of this line is approximately the same as for the strongest $5d$–$6p$ and $6s$–$6p$ transitions. The increased uncertainty from the correction factor k_1 includes the errors caused

Table 1. Lifetimes, branching fractions and transition probabilities in Yb III.

Level		σ_{Ritz}	BF_k	$u(BF_k)^a$	A_k	$u(A_k)^b$	$\log gf$		Source[d]
upper	lower	(cm^{-1})		(%)	(10^7 s^{-1})	(%)	This work[c]	Ref. [3]	
$6p\,(7/2,1/2)_3$	$5d\,(5/2,3/2)^\circ_4$	25083.459	0.039	20	0.017	4	–2.54	–2.39	B
72140.434	$5d\,(7/2,5/2)^\circ_3$	29121.207	0.085	19	0.037	20	–2.33	–2.09	B
$\tau = 2.28$ ns	$5d\,(7/2,5/2)^\circ_2$	31852.326	1.26	6	0.56	10	–1.24	–1.21	B
$r_1^e = 0.124$	$5d\,(7/2,3/2)^\circ_4$	31980.342[g]	7.7	6	3.4	10	–0.46	–0.50	B
$r_2^f = 0.14$	$5d\,(7/2,3/2)^\circ_3$	32999.226	11.4	5	5.0	9	–0.31	–0.28	A, B
	$6s\,(7/2,1/2)^\circ_3$	37149.722	7.51	1.7	3.3	8	–0.60	–0.59	A
	$6s\,(7/2,1/2)^\circ_4$	37484.203[h]	54.8	1.3	24.0	8	0.25	0.28	A
	$5d\,(7/2,3/2)^\circ_2$	38754.573	17	1.8	7.5	8	–0.29	–0.30	A
$6p\,(7/2,1/2)_4$	$5d\,(5/2,3/2)^\circ_4$	25430.078	0.122	13	0.055	15	–1.94	–1.90	B
72487.053	$5d\,(7/2,5/2)^\circ_5$	28864.220	0.20	11	0.092	14	–1.82	–2.04	B
$\tau = 2.22$ ns	$5d\,(7/2,5/2)^\circ_3$	29467.826	0.124	14	0.056	16	–2.06	–2.17	B
$r_1^e = 0.032$	$5d\,(7/2,5/2)^\circ_4$	30061.926	0.92	9	0.45	12	–1.21	–1.35	B
$r_2^f = 0.044$	$5d\,(7/2,3/2)^\circ_4$	32326.961[g]	3.6	14	1.6	16	–0.68	–0.37	A
	$5d\,(7/2,3/2)^\circ_3$	33345.845	3.1	7.6	1.41	11	–0.77	–0.92	A, B
	$5d\,(7/2,3/2)^\circ_5$	35466.669[h]	25.8	1.4	11.6	8	0.09	0.06	A, E
	$6s\,(7/2,1/2)^\circ_3$	37496.342	43.3	1.4	19.5	8	0.27	0.28	A
	$6s\,(7/2,1/2)^\circ_4$	37830.822	22.7	2	10.2	8	–0.02	–0.01	E
$6p\,(7/2,3/2)_5$	$5d\,(5/2,5/2)^\circ_5$	27663.120	0.080	19	0.052	20	–1.94	–1.99	B
78020.641	$5d\,(7/2,5/2)^\circ_5$	34397.807	5.7	7	3.7	10	–0.28	–0.34	A, B
$\tau = 1.53$ ns	$5d\,(7/2,5/2)^\circ_4$	35595.513	0.69	10	0.45	13	–1.23	–1.59	A
$r_1^e = 0.065$	$5d\,(7/2,3/2)^\circ_4$	37860.549	1.85	5	1.20	9	–0.86	–1.00	A
$r_2^f = 0.0013$	$5d\,(7/2,5/2)^\circ_6$	38935.166[h]	25.8	3	16.9	8	0.26	0.24	A
	$5d\,(7/2,3/2)^\circ_5$	41000.256	1.33	3	0.87	9	–1.07	–1.00	A
	$6s\,(7/2,1/2)^\circ_4$	43364.409[g]	64.4	1.0	42	8	0.56	0.60	A
$6p\,(7/2,3/2)_2$	$5d\,(5/2,3/2)^\circ_1$	24818.302	1.04	8	0.71	11	–1.06	–1.11	B
78183.527	$5d\,(5/2,5/2)^\circ_1$	28154.057	0.36	15	0.25	17	–1.63	–1.68	B
$\tau = 1.48$ ns	$5d\,(7/2,5/2)^\circ_3$	35164.300	5.1	7	3.5	10	–0.68	–0.72	A
$r_1^e = 0.884$	$5d\,(7/2,5/2)^\circ_2$	37895.419[h]	13.6	4	9.2	9	–0.32	–0.37	A, B
$r_2^f = 0.33$	$5d\,(7/2,5/2)^\circ_1$	38462.689	9.9	4	6.7	9	–0.47	–0.52	A
	$5d\,(7/2,3/2)^\circ_3$	39042.319	0.73	8	0.49	11	–1.61	–1.94	A
	$6s\,(7/2,1/2)^\circ_3$	43192.816[g]	69	9	46	12	0.27	0.27	A
	$5d\,(7/2,3/2)^\circ_2$	44797.666	0.47	19	0.32	20	–1.92	–2.16	A
$6p\,(7/2,3/2)_3$	$5d\,(5/2,5/2)^\circ_3$	25656.404	0.14	20	0.10	20	–1.79	–1.97	B
78779.259	$5d\,(7/2,5/2)^\circ_3$	35760.033[g]	12.7	5	9.1	10	–0.13	–0.20	A, B
$\tau = 1.41$ ns	$5d\,(7/2,5/2)^\circ_4$	36354.132	13.7	5	9.8	9	–0.11	–0.20	A
$r_1^e = 0.802$	$5d\,(7/2,5/2)^\circ_2$	38491.151	3.95	4	2.8	9	–0.71	–0.80	A
$r_2^f = 0.39$	$5d\,(7/2,3/2)^\circ_4$	38619.167	0.73	7	0.51	10	–1.44	–1.38	A
	$5d\,(7/2,3/2)^\circ_3$	39638.051	0.20	16	0.14	18	–2.02	–2.52	A
	$6s\,(7/2,1/2)^\circ_3$	43788.548[h]	56.1	1.2	40	8	0.34	0.33	A
	$6s\,(7/2,1/2)^\circ_4$	44123.028	8.57	1.6	6.1	8	–0.49	–0.46	A
	$5d\,(7/2,3/2)^\circ_2$	45393.398	3.70	3	2.6	8	–0.88	–0.90	A
$6p\,(7/2,3/2)_4$	$5d\,(7/2,5/2)^\circ_5$	35660.145	14.1	6	10.1	10	0.03	–0.02	A
79282.979	$5d\,(7/2,5/2)^\circ_3$	36263.752	1.19	8	0.85	11	–1.06	–1.20	A
$\tau = 1.40$ ns	$5d\,(7/2,5/2)^\circ_4$	36857.851[g]	6.7	6	4.8	10	–0.33	–0.36	A
$r_1^e = 0.364$	$5d\,(7/2,3/2)^\circ_4$	39122.887	3.12	4	2.2	9	–0.71	–0.67	A
$r_2^f = 0.16$	$5d\,(7/2,3/2)^\circ_3$	40141.770	3.20	4	2.3	9	–0.72	–0.68	A
	$5d\,(7/2,3/2)^\circ_5$	42262.594	2.73	3	1.95	8	–0.83	–0.90	A
	$6s\,(7/2,1/2)^\circ_3$	44292.267[h]	23.6	1.4	16.8	8	0.06	0.06	A
	$6s\,(7/2,1/2)^\circ_4$	44626.748	45.2	1.2	32	8	0.34	0.34	A

Table 1. *Continued.*

Level		σ_{Ritz}	BF_k	$u(BF_k)^a$	A_k	$u(A_k)^b$	$\log gf$		Source[d]
upper	lower	(cm^{-1})		(%)	(10^7 s^{-1})	(%)	This work[c]	Ref. [3]	
$6p\,(5/2,1/2)_3$	$5d\,(5/2,5/2)^\circ_3$	29423.534	0.26	20	0.12	20	–1.83	–2.51	B
82546.389	$5d\,(5/2,3/2)^\circ_3$	30964.535[g]	7.9	5	3.7	9	–0.39	–0.41	B
$\tau = 2.11$ ns	$5d\,(5/2,3/2)^\circ_2$	34131.682	3.5	10	1.6	13	–0.83	–1.04	A
$r_1^e = 0.331$	$5d\,(5/2,3/2)^\circ_4$	35489.414	24.8	3	11.7	9	–0.01	–0.04	A, B
$r_2^f = 0.52$	$6s\,(5/2,1/2)^\circ_3$	37338.717	19.7	3	9.4	9	–0.15	–0.14	A, E
	$6s\,(5/2,1/2)^\circ_2$	37692.791[h]	41.4	4	19.6	9	0.16	0.15	E
	$5d\,(7/2,5/2)^\circ_3$	39527.162	0.41	12	0.20	14	–1.88	–2.17	A
	$5d\,(7/2,5/2)^\circ_4$	40121.261	0.35	15	0.17	17	–1.96	–1.70	A
	$5d\,(7/2,5/2)^\circ_2$	42258.281	0.20	19	0.094	20	–2.25	–3.06	D
	$5d\,(7/2,3/2)^\circ_4$	42386.297	0.37	18	0.17	20	–1.99	–2.08	A, D
	$5d\,(7/2,3/2)^\circ_3$	43405.181	0.40	19	0.19	20	–1.97	–3.98	A
	$6s\,(7/2,1/2)^\circ_3$	47555.677	0.56	20	0.27	20	–1.9	–2.05	D
$6p\,(5/2,1/2)_2$	$5d\,(5/2,3/2)^\circ_1$	29542.271[h]	7.2	5	3.1	10	–0.58	–0.58	B
82907.497	$5d\,(5/2,3/2)^\circ_3$	31325.643[g]	7.5	5	3.2	9	–0.61	–0.65	B
$\tau = 2.35$ ns	$5d\,(5/2,5/2)^\circ_1$	32878.026	0.69	30	0.29	30	–1.69	–1.78	B
$r_1^e = 0.571$	$5d\,(5/2,3/2)^\circ_2$	34492.790	13.2	3	5.6	9	–0.45	–0.41	A, B
$r_2^f = 0.36$	$6s\,(5/2,1/2)^\circ_3$	37699.825	56.8	1.6	24.1	8	0.10	0.15	A
	$6s\,(5/2,1/2)^\circ_2$	38053.899	9.0	3	3.8	9	–0.71	–0.71	A
	$5d\,(7/2,5/2)^\circ_3$	39888.270	1.61	7	0.69	10	–1.49	–1.81	A
	$5d\,(7/2,5/2)^\circ_2$	42619.389	0.23	11	0.097	14	–2.4	–2.92	C
	$5d\,(7/2,5/2)^\circ_1$	43186.659	3.1	7	1.31	11	–1.28	–1.27	A, C
	$5d\,(7/2,3/2)^\circ_3$	43766.289	0.18	14	0.076	16	–2.52	–3.21	C
	$6s\,(7/2,1/2)^\circ_3$	47916.785	0.44	20	0.19	30	–2.21	–2.30	C
$6p\,(5/2,3/2)_1$	$5d\,(5/2,5/2)^\circ_2$	36149.257	11.1	6	8.0	10	–0.56	–0.69	A
87612.643	$5d\,(5/2,5/2)^\circ_1$	37583.172	14.4	4	10.3	9	–0.49	–0.56	A
$\tau^i = 1.40$ ns	$5d\,(5/2,3/2)^\circ_2$	39197.935	1.4	15	0.99	17	–1.54	–1.73	A
$r_1^e = 0.097$	$5d\,(5/2,5/2)^\circ_0$	42191.597	8.6	3	6.1	9	–0.82	–0.87	A, C
$r_2^f = 0.076$	$6s\,(5/2,1/2)^\circ_2$	42759.045	62.8	1.1	45	8	0.04	0.04	A
	$5d\,(7/2,5/2)^\circ_1$	47891.805	1.6	17	1.2	19	–1.64	–1.73	C
$6p\,(5/2,3/2)_4$	$5d\,(5/2,5/2)^\circ_4$	34762.044	5.3	8	3.1	12	–0.46	–0.44	A
88497.973	$5d\,(5/2,5/2)^\circ_3$	35375.118	0.22	15	0.14	17	–1.83	–1.81	D
$\tau = 1.67$ ns	$5d\,(5/2,3/2)^\circ_3$	36916.119	0.48	20	0.29	20	–1.54	–1.56	A
$r_1^e = 0.473$	$5d\,(5/2,5/2)^\circ_5$	38140.452[h]	25.2	3	15.1	9	0.14	0.16	A
$r_2^f = 0.23$	$5d\,(5/2,3/2)^\circ_4$	41440.998	1.32	6	0.80	10	–1.20	–1.14	A, D
	$6s\,(5/2,1/2)^\circ_3$	43290.301[g]	65.0	1.1	39	8	0.44	0.52	A
	$5d\,(7/2,5/2)^\circ_5$	44875.140	0.61	20	0.36	20	–1.61	–1.76	A
	$5d\,(7/2,5/2)^\circ_3$	45478.746	1.7	8	1.00	12	–1.18	–1.48	A
	$5d\,(7/2,5/2)^\circ_4$	46072.846	0.13	20	0.079	20	–2.3	–2.16	D
$6p\,(5/2,3/2)_2$	$5d\,(5/2,3/2)^\circ_1$	35611.936	0.75	8	0.52	11	–1.51	–1.40	D
88977.161	$5d\,(5/2,5/2)^\circ_3$	35854.306	13.6	4	9.5	9	–0.26	–0.33	A, D
$\tau^i = 1.43$ ns	$5d\,(5/2,3/2)^\circ_3$	37395.307	1.65	10	1.15	13	–1.21	–1.00	A
$r_1^e = 0.225$	$5d\,(5/2,5/2)^\circ_2$	37513.775	10.5	4	7.4	9	–0.41	–0.41	A
$r_2^f = 0$	$5d\,(5/2,5/2)^\circ_1$	38947.691	3.03	6	2.1	10	–0.98	–1.10	A
	$5d\,(5/2,3/2)^\circ_2$	40562.454	0.70	16	0.49	18	–1.65	–2.39	A
	$6s\,(5/2,1/2)^\circ_3$	43769.489	8.3	6	5.8	10	–0.65	–0.62	A, D
	$6s\,(5/2,1/2)^\circ_2$	44123.564	59.3	2	42	8	0.20	0.20	A
	$5d\,(7/2,5/2)^\circ_3$	45957.934	0.12	30	0.086	30	–2.51	–3.13	D
	$5d\,(7/2,5/2)^\circ_1$	49256.323	1.9	20	1.3	20	–1.38	–1.59	D

Table 1. *Continued.*

Level		σ_{Ritz}	BF_k	$u(BF_k)^a$	A_k	$u(A_k)^b$	$\log gf$		Source[d]
upper	lower	(cm^{-1})		(%)	(10^7 s^{-1})	(%)	This work[c]	Ref. [3]	
$6p\,(5/2,3/2)_3$	$5d\,(5/2,5/2)^\circ_4$	35661.532	15.7	6	11.8	10	–0.01	–0.10	A
89397.462	$5d\,(5/2,5/2)^\circ_3$	36274.607	7.0	6	5.3	10	–0.38	–0.38	A
$\tau^i = 1.32$ ns	$5d\,(5/2,3/2)^\circ_3$	37815.608	4.7	6	3.5	10	–0.59	–0.91	A
$r_1^e = 0.324$	$5d\,(5/2,5/2)^\circ_2$	37934.076	2.29	7	1.73	11	–0.90	–1.30	A
$r_2^f = 0.32$	$5d\,(5/2,3/2)^\circ_2$	40982.755	1.96	6	1.49	10	–1.03	–0.93	A
	$5d\,(5/2,3/2)^\circ_4$	42340.487	2.59	5	1.96	9	–0.94	–0.97	A
	$6s\,(5/2,1/2)^\circ_3$	44189.790	37.7	1.4	29	8	0.18	0.18	A
	$6s\,(5/2,1/2)^\circ_2$	44543.864	25.2	1.5	19.1	8	0.00	–0.03	A, C
	$5d\,(7/2,5/2)^\circ_3$	46378.235	2.70	3	2.05	9	–1.00	–1.16	C
$7s\,(7/2,1/2)^\circ_4$	$6p\,(7/2,3/2)_4$	40964.125	20.5	4	16.6	9	0.12	0.13	D
120247.103	$6p\,(7/2,3/2)_3$	41467.844	3.4	13	2.8	15	–0.66	–0.77	D
$\tau^i = 1.24$ ns	$6p\,(7/2,3/2)_5$	42226.463	38.7	4	31	9	0.37	0.37	D
$r_1^e = 12.1$	$6p\,(7/2,1/2)_4$	47760.050	11.3	17	9.2	19	–0.27	–0.10	D
$r_2^f = 0.047$	$6p\,(7/2,1/2)_3$	48106.669	26	9	21	12	0.08	0.16	D
$7s\,(7/2,1/2)^\circ_3$	$6p\,(7/2,3/2)_4$	41081.880	15.7	5	11.6	9	–0.14	–0.18	D
120364.858	$6p\,(7/2,3/2)_3$	41585.599	29.1	4	21.4	9	0.11	0.11	D
$\tau^i = 1.36$ ns	$6p\,(7/2,3/2)_2$	42181.331	26.1	4	19.2	9	0.05	0.03	D
$r_1^e = 23.5$	$6p\,(7/2,1/2)_4$	47877.805	29	8	21	11	–0.02	0.16	D
$r_2^f = 6.4$									
$7s\,(5/2,1/2)^\circ_2$	$6p\,(5/2,3/2)_3$	41060.095	18	14	16	16	–0.14	–0.28	D
130457.557	$6p\,(5/2,3/2)_2$	41480.396	26	13	24	15	0.01	–0.01	D
$\tau^i = 1.08$ ns	$6p\,(5/2,3/2)_1$	42844.914	21	14	19	16	–0.11	–0.21	D
$r_1^e = 59.6$	$6p\,(5/2,1/2)_3$	47911.168	36	18	33	20	0.03	0.03	D
$r_2^f = 6.4$									
$7s\,(5/2,1/2)^\circ_3$	$6p\,(5/2,3/2)_3$	41153.729	22	10	13.3	13	–0.09		D
130551.191	$6p\,(5/2,3/2)_2$	41574.030	4.6	40	2.8	40	–0.78	–0.92	D
$\tau^i = 1.66$ ns	$6p\,(5/2,3/2)_4$	42053.218	55	7	33	11	0.29	0.29	D
$r_1^e = 64.0$	$6p\,(5/2,1/2)_2$	47643.694	18	30	11	30	–0.30	0.03	D
$r_2^f = 16.7$									

[a] Relative uncertainties. [b] Relative uncertainties estimated by $u(A_k) = (u(BF_k)^2 + 8^2)^{1/2}$. [c] Calculated by the definition in [17]. [d] Indicates the discharge current and source BF_k was measured in: 0.30 A (A), 0.60 A (B) 0.90 A (C) 1.02 A (D) in the PD and 0.44 A (E) in the HC. Transitions with two indices are normalization lines between spectra. [e] Experimental residual of BF_k due to missing lines. [f] Semi-empirical residual of BF_k due to missing lines derived from [3]. [g] Pump channel. [h] Fluorescence channel. [i] Lifetime derived from the semi-empirical A-value from [3] of the strongest transition.

by self-absorption in these transitions. Furthermore, the uncertainty u_{obs} of the measured wavenumber of the resonance transition is close to those of the $5d$–$6p$ and $6s$–$6p$ transitions. The largest part of the systematic level shift caused by the self-absorption of the 39 721 cm^{-1} line should, therefore, be covered by the increased uncertainty from the k_1 factor.

The resulting level energies of Yb III from the least-squares fit are presented in Table 2. Compared with prior values [4], the accuracy of the fitted absolute level energies has been improved by about an order of magnitude. Of the 11 new levels suggested in [3] three $6d$ levels have been verified. Note that two of these are only defined by one observed transition. When comparing PD and HC-spectra the intensities and line shapes for all transitions singularly defining a $6d$ level behave, however, as all other transitions from levels above 120 000 cm^{-1}.

Another level defined by only one observed transition is $5d\,(5/2{,}5/2)^\circ_0$. In previous works the stated energy of this level was 46157.66 cm^{-1} [19] and 45 276.85 cm^{-1} [4,20]. This level is connected to the rest of the system through the $6p\,(5/2{,}3/2)_1$ level, which, in work prior to this, has been given the energy 87 612.61 cm^{-1} [4]. From the semi-empirically calculated A-values [3] a S/N of about 200 was expected in the PD-spectra for the transition defining the $5d$ level. No lines were, however, found at the positions predicted by any of the two level energies. Instead, by comparing PD and HC spectra from different discharge conditions, a spectral line at 42 191.597 cm^{-1} was found to have both an intensity and a line shape that

Table 2. Fitted energy levels in Yb III.

Config.[a]	Term	J	Energy (cm^{-1})	u(E) (10^{-3})	l[b]
$4f^{14}$	^{1}S	0	0	0	3
$(^2F^\circ_{7/2})5d_{3/2}$	(7/2,3/2)°	2	33385.8613	1.6	3
		5	37020.3842	1.5	3
		3	39141.2082	1.6	6
		4	40160.0920	1.5	6
$(^2F^\circ_{7/2})6s_{1/2}$	(7/2,1/2)°	4	34656.2310	1.5	4
		3	34990.7117	1.4	7
$(^2F^\circ_{7/2})5d_{5/2}$	(7/2,5/2)°	6	39085.4741	1.6	1
		1	39720.8382	0.3	5
		2	40288.1079	1.6	5
		4	42425.1278	1.7	5
		3	43019.2268	1.6	12
		5	43622.8333	1.8	4
$(^2F^\circ_{5/2})6s_{1/2}$	(5/2,1/2)°	2	44853.5977	1.8	4
		3	45207.672	2	4
$(^2F^\circ_{5/2})5d_{5/2}$	(5/2,5/2)°	0	45421.045[c]	3	1
		1	50029.4707	1.7	5
		5	50357.521	2	1
		2	51463.386	2	3
		3	53122.856	2	5
		4	53735.930	3	2
$(^2F^\circ_{5/2})5d_{3/2}$	(5/2,3/2)°	4	47056.976	2	5
		2	48414.707	2	6
		3	51581.854	2	4
		1	53365.226	3	4
$(^2F^\circ_{7/2})6p_{1/2}$	(7/2,1/2)	3	72140.4342	1.5	10
		4	72487.0533	1.4	10
$(^2F^\circ_{7/2})6p_{3/2}$	(7/2,3/2)	5	78020.6405	1.6	6
		2	78183.5272	1.4	11
		3	78779.2594	1.5	14
		4	79282.9785	1.5	12
$(^2F^\circ_{5/2})6p_{1/2}$	(5/2,1/2)	3	82546.389	2	11
		2	82907.4969	1.6	11
$(^2F^\circ_{5/2})6p_{3/2}$	(5/2,3/2)	1	87612.6428	1.8	7
		4	88497.973	2	10
		2	88977.161	2	14
		3	89397.4620	1.9	15
$(^2F^\circ_{7/2})7s_{1/2}$	(7/2,1/2)°	4	120247.103	3	5
		3	120364.858	4	4
$(^2F^\circ_{7/2})6d_{3/2}$	(7/2,3/2)°	3	125560.54[d]	60	1
		4	125810.11	40	1
$(^2F^\circ_{7/2})6d_{5/2}$	(7/2,5/2)°	6	125731.113[d]	11	1
		2	125987.08	20	2
		4	126456.119	13	2
		3	126559.21	20	2
		5	126671.590[d]	17	2
$(^2F^\circ_{5/2})7s_{1/2}$	(5/2,1/2)°	2	130457.557	11	4
		3	130551.191	8	4
$(^2F^\circ_{5/2})6d_{5/2}$	(5/2,5/2)°	2	136350.97	30	1
		3	136699.79	30	2
		4	136849.59	30	1

[a] Level assignment of [4]. Apart from the ground state, the level system is best described in J_1j-coupling [18]. [b] Number of observed transitions connected to the level. [c] The energy of this level has been increased by 144.20 cm^{-1} from the previous value in [4]. [d] Levels identified in [3].

behaved as an Yb III transition from a $6p$ level. This line also had the expected S/N, while all other possible candidates had a S/N that was more than an order of magnitude too small. In addition to this, the branching ratios formed by the 42 191.597 cm^{-1} line and the other transitions from the $6p\,(5/2,3/2)_1$ level remained constant between PD-spectra sampled at different discharge currents. There is also a good agreement between the A-value for the 42 191.597 cm^{-1} derived in this work and corresponding value in [3], which can be seen in the comparison of the $\log gf$ values in Table 1.

The earlier misidentifications probably have an explanation in spectra contaminated by other elements, while the use of aluminum for the cathode insets in this work kept the number of unwanted lines in the PD-spectra low. As a comparison with earlier works, in [21] the 42 191.597 cm^{-1} line was identified as an Yb II transition, while in [19] it was identified as an unclassified Yb III transition. In [19] the theoretically derived energy of the $5d\,(5/2,5/2)^\circ_0$ level is 45 761 cm^{-1}, which is closer to the new energy of 45 421.045 cm^{-1} derived in the present work than to both of the prior values.

Apart from the $5d\,(5/2,5/2)^\circ_0$ level, there are no large systematic deviations between the level energies presented here and those in investigations prior to this work. The error bars of the latter cover the differences. Further, new energy levels were sought for, but none was found. This means that the ionization energy of Yb III, which has been determined to $202.07(20) \times 10^3$ cm^{-1} [22], cannot be improved.

The level energies in Table 2 can be viewed as the mean of energies of the individual isotopes, where the contribution from each isotope is weighted by its relative abundance. This interpretation is possible since the wavenumbers have been measured as the center of gravity of the line profiles. Note that neither hfs, nor Zeeman splitting influences the center of gravity of the individual isotope components in the profiles.

Table 3. Finding list for observed Yb III transitions.

σ_{Ritz} (cm^{-1})	u_{Ritz}	u_{obs} (10^{-3} cm^{-1})	$(\sigma_{Ritz} - \sigma_{obs})$	log I^a	log gf^b	Transition lower	Transition upper	λ^c (Å)	Source^d
23725.7268	2.3	23	5.5			$5d\,(5/2,3/2)^{\circ}_{2}$	$6p\,(7/2,1/2)_{3}$	4213.6470	F
24818.3016	2.7	4.1	–7.3		–1.06	$5d\,(5/2,3/2)^{\circ}_{1}$	$6p\,(7/2,3/2)_{2}$	4028.1462	F
25083.4586	2.2	15	1.6		–2.54	$5d\,(5/2,3/2)^{\circ}_{4}$	$6p\,(7/2,1/2)_{3}$	3985.5638	F
25430.0778	2.2	9.8	1.4		–1.94	$5d\,(5/2,3/2)^{\circ}_{4}$	$6p\,(7/2,1/2)_{4}$	3931.2382	F
25656.4039	2.2	22	–12		–1.79	$5d\,(5/2,5/2)^{\circ}_{3}$	$6p\,(7/2,3/2)_{3}$	3896.5583	F
28154.0565	1.9	14	2.6		–1.63	$5d\,(5/2,5/2)^{\circ}_{1}$	$6p\,(7/2,3/2)_{2}$	3550.8716	F
28864.2199	1.1	7.9	–11		–1.82	$5d\,(7/2,5/2)^{\circ}_{5}$	$6p\,(7/2,1/2)_{4}$	3463.5049	F
29121.2073	1.1	21	< 0.1		–2.33	$5d\,(7/2,5/2)^{\circ}_{3}$	$6p\,(7/2,1/2)_{3}$	3432.9394	F
29423.5336	2.0	17	–8.3		–1.83	$5d\,(5/2,5/2)^{\circ}_{3}$	$6p\,(5/2,1/2)_{3}$	3397.6649	F
29467.8264	1.1	14	2.3		–2.06	$5d\,(7/2,5/2)^{\circ}_{3}$	$6p\,(7/2,1/2)_{4}$	3392.5577	F
29542.2713	2.3	2.0	1.0		–0.58	$5d\,(5/2,3/2)^{\circ}_{1}$	$6p\,(5/2,1/2)_{2}$	3384.0084	F
30061.9255	1.0	2.7	–4.1		–1.21	$5d\,(7/2,5/2)^{\circ}_{4}$	$6p\,(7/2,1/2)_{4}$	3325.5101	F
30964.5347	1.9	1.8	–1.9		–0.39	$5d\,(5/2,3/2)^{\circ}_{3}$	$6p\,(5/2,1/2)_{3}$	3228.5690	F
31325.6425	2.2	2.5	–0.5		–0.61	$5d\,(5/2,3/2)^{\circ}_{3}$	$6p\,(5/2,1/2)_{2}$	3191.3502	F
31852.3262	0.9	2.9	–5.2		–1.24	$5d\,(7/2,5/2)^{\circ}_{2}$	$6p\,(7/2,1/2)_{3}$	3138.5787	F
31980.3422	0.5	0.6	–1.1		–0.46	$5d\,(7/2,3/2)^{\circ}_{4}$	$6p\,(7/2,1/2)_{3}$	3126.0147	F
32326.9613	0.6	0.7	–1.6		–0.68	$5d\,(7/2,3/2)^{\circ}_{4}$	$6p\,(7/2,1/2)_{4}$	3092.4953	F
32878.0262	1.8	47	–28		–1.69	$5d\,(5/2,5/2)^{\circ}_{1}$	$6p\,(5/2,1/2)_{2}$	3040.6603	F
32999.2260	0.6	0.6	–1.4		–0.32	$5d\,(7/2,3/2)^{\circ}_{3}$	$6p\,(7/2,1/2)_{3}$	3029.4921	F
33345.8451	0.7	1.9	–1.8		–0.77	$5d\,(7/2,3/2)^{\circ}_{3}$	$6p\,(7/2,1/2)_{4}$	2998.0002	F
34131.6817	2.2	5.6	2.5	2.86	–0.83	$5d\,(5/2,3/2)^{\circ}_{2}$	$6p\,(5/2,1/2)_{3}$	2928.9722	B
34397.8071	1.1	1.5	–0.8	3.45	–0.28	$5d\,(7/2,5/2)^{\circ}_{5}$	$6p\,(7/2,3/2)_{5}$	2906.3106	B
34492.7895	1.7	1.6	–0.9	3.23	–0.45	$5d\,(5/2,3/2)^{\circ}_{2}$	$6p\,(5/2,1/2)_{2}$	2898.3072	B
34762.0435	2.1	2.0	–1.1	2.86	–0.46	$5d\,(5/2,5/2)^{\circ}_{4}$	$6p\,(5/2,3/2)_{4}$	2875.8569	C
35164.3003	1.1	1.4	0.2	3.03	–0.68	$5d\,(7/2,5/2)^{\circ}_{3}$	$6p\,(7/2,3/2)_{2}$	2842.9574	C
35375.1177	2.0	20	1.3	1.54	–1.83	$5d\,(5/2,5/2)^{\circ}_{3}$	$6p\,(5/2,3/2)_{4}$	2826.0140	D
35466.6691	0.4	0.3	< 0.1	4.22	0.09	$5d\,(7/2,3/2)^{\circ}_{5}$	$6p\,(7/2,1/2)_{4}$	2818.7188	A
35489.4136	1.2	1.0	–0.8	3.69	–0.01	$5d\,(5/2,3/2)^{\circ}_{4}$	$6p\,(5/2,1/2)_{3}$	2816.9122	A
35595.5127	1.1				–1.23	$5d\,(7/2,5/2)^{\circ}_{4}$	$6p\,(7/2,3/2)_{5}$	2808.5155	G
35611.9356	2.9	7.9	9.7	1.73	–1.51	$5d\,(5/2,3/2)^{\circ}_{1}$	$6p\,(5/2,3/2)_{2}$	2807.2202	D
35660.1452	1.0	0.9	0.6	3.67	0.03	$5d\,(7/2,5/2)^{\circ}_{5}$	$6p\,(7/2,3/2)_{4}$	2803.4249	A
35661.5322	2.1	2.2	1.2	3.17	–0.01	$5d\,(5/2,5/2)^{\circ}_{4}$	$6p\,(5/2,3/2)_{3}$	2803.3159	A
35760.0326	1.0	1.2	0.8	3.54	–0.13	$5d\,(7/2,5/2)^{\circ}_{3}$	$6p\,(7/2,3/2)_{3}$	2795.5938	A
35854.3057	1.2	1.0	0.4	2.98	–0.26	$5d\,(5/2,5/2)^{\circ}_{3}$	$6p\,(5/2,3/2)_{2}$	2788.2429	C
36149.2567	1.7	1.7	3.8	2.70	–0.56	$5d\,(5/2,5/2)^{\circ}_{2}$	$6p\,(5/2,3/2)_{1}$	2765.4917	C
36263.7517	1.1	2.0	0.4	2.59	–1.06	$5d\,(7/2,5/2)^{\circ}_{3}$	$6p\,(7/2,3/2)_{4}$	2756.7598	C
36274.6065	1.6	1.7	–1.1	2.83	–0.38	$5d\,(5/2,5/2)^{\circ}_{3}$	$6p\,(5/2,3/2)_{3}$	2755.9348	B
36354.1317	1.0	0.9	0.3	3.56	–0.11	$5d\,(7/2,5/2)^{\circ}_{4}$	$6p\,(7/2,3/2)_{3}$	2749.9059	A
36857.8507	1.0	1.2	0.2	3.33	–0.33	$5d\,(7/2,5/2)^{\circ}_{4}$	$6p\,(7/2,3/2)_{4}$	2712.3222	A
36916.1188	2.1	6.5	4.9	1.88	–1.54	$5d\,(5/2,3/2)^{\circ}_{3}$	$6p\,(5/2,3/2)_{4}$	2708.0408	C
37149.7225	0.6	1.0	0.3	3.58	–0.60	$6s\,(7/2,1/2)^{\circ}_{3}$	$6p\,(7/2,1/2)_{3}$	2691.0113	A
37338.7167	1.1	1.0	1.3	3.56	–0.15	$6s\,(5/2,1/2)^{\circ}_{3}$	$6p\,(5/2,1/2)_{3}$	2677.3896	A
37395.3067	2.3	3.9	8.4	2.02	–1.21	$5d\,(5/2,3/2)^{\circ}_{3}$	$6p\,(5/2,3/2)_{2}$	2673.3377	C
37484.2031	0.3	0.3	0.6	4.42	0.25	$6s\,(7/2,1/2)^{\circ}_{4}$	$6p\,(7/2,1/2)_{3}$	2666.9973	A
37496.3416	0.3	0.3	0.3	4.41	0.27	$6s\,(7/2,1/2)^{\circ}_{3}$	$6p\,(7/2,1/2)_{4}$	2666.1339	A
37513.7751	1.3	1.1	–1.8	2.83	–0.41	$5d\,(5/2,5/2)^{\circ}_{2}$	$6p\,(5/2,3/2)_{2}$	2664.8948	B
37583.1721	1.4	1.3	–1.8	2.78	–0.49	$5d\,(5/2,5/2)^{\circ}_{1}$	$6p\,(5/2,3/2)_{1}$	2659.9739	B
37692.7914	2.0				0.16	$6s\,(5/2,1/2)^{\circ}_{2}$	$6p\,(5/2,1/2)_{3}$	2652.2376	G
37699.8245	1.9				0.10	$6s\,(5/2,1/2)^{\circ}_{3}$	$6p\,(5/2,1/2)_{2}$	2651.7428	G
37700.7142	3.7					$6p\,(5/2,1/2)_{3}$	$7s\,(7/2,1/2)^{\circ}_{4}$	2651.6802	G
37815.6075	2.1				–0.59	$5d\,(5/2,3/2)^{\circ}_{3}$	$6p\,(5/2,3/2)_{3}$	2643.6232	G
37830.8223	0.6				–0.02	$6s\,(7/2,1/2)^{\circ}_{4}$	$6p\,(7/2,1/2)_{4}$	2642.5600	G
37860.5485	0.6	0.9	1.3	2.91	–0.86	$5d\,(7/2,3/2)^{\circ}_{4}$	$6p\,(7/2,3/2)_{5}$	2640.4850	B
37895.4192	0.8	0.9	–0.2	3.40	–0.32	$5d\,(7/2,5/2)^{\circ}_{2}$	$6p\,(7/2,3/2)_{2}$	2638.0552	A
37934.0759	1.8	3.3	0.5	2.13	–0.90	$5d\,(5/2,5/2)^{\circ}_{2}$	$6p\,(5/2,3/2)_{3}$	2635.3667	C
38053.8992	1.2	1.1	–0.6	3.01	–0.71	$6s\,(5/2,1/2)^{\circ}_{2}$	$6p\,(5/2,1/2)_{2}$	2627.0680	B
38140.4522	0.9	0.7		3.48	0.14	$5d\,(5/2,5/2)^{\circ}_{5}$	$6p\,(5/2,3/2)_{4}$	2621.1060	A

Table 3. *Continued.*

σ_{Ritz} (cm^{-1})	u_{Ritz}	u_{obs} (10^{-3} cm^{-1})	$(\sigma_{Ritz} - \sigma_{obs})$	$\log I^a$	$\log gf^b$	Transition lower	Transition upper	λ^c (Å)	Source[d]
38462.6889	1.3	1.1	–0.6	3.25	–0.47	$5d\,(7/2,5/2)^\circ_1$	$6p\,(7/2,3/2)_2$	2599.1453	A
38491.1515	0.8	0.7	0.5	2.99	–0.71	$5d\,(7/2,5/2)^\circ_2$	$6p\,(7/2,3/2)_3$	2597.2232	B
38619.1674	0.7	2.3	4.6	2.27	–1.44	$5d\,(7/2,3/2)^\circ_4$	$6p\,(7/2,3/2)_3$	2588.6133	C
38754.5729	0.4	0.3	< 0.1	3.90	–0.29	$5d\,(7/2,3/2)^\circ_2$	$6p\,(7/2,1/2)_3$	2579.5683	A
38935.1664	0.4	0.3		4.02	0.26	$5d\,(7/2,5/2)^\circ_6$	$6p\,(7/2,3/2)_5$	2567.6027	A
38947.6905	2.0	3.4	3.0	2.23	–0.98	$5d\,(5/2,5/2)^\circ_1$	$6p\,(5/2,3/2)_2$	2566.7770	B
39042.3190	0.9	3.4	1.1	2.08	–1.61	$5d\,(7/2,3/2)^\circ_3$	$6p\,(7/2,3/2)_2$	2560.5554	C
39122.8866	0.6	0.7	1.9	2.97	–0.71	$5d\,(7/2,3/2)^\circ_4$	$6p\,(7/2,3/2)_4$	2555.2820	B
39197.9354	2.1	6.3	–7.3	1.82	–1.54	$5d\,(5/2,3/2)^\circ_2$	$6p\,(5/2,3/2)_1$	2550.3893	C
39527.1623	2.0	5.9	–6.8	1.82	–1.88	$5d\,(7/2,5/2)^\circ_3$	$6p\,(5/2,1/2)_3$	2529.1454	C
39638.0512	0.8	8.3	–7.4	1.55	–2.02	$5d\,(7/2,3/2)^\circ_3$	$6p\,(7/2,3/2)_3$	2522.0696	C
39720.8382	0.3	0.2	< 0.1	4.44		$4f^{\,14}\,{}^1\mathrm{S}_0$	$5d\,(7/2,5/2)^\circ_1$	2516.8127	A
39888.2701	1.8	3.3	–5.4	2.23	–1.49	$5d\,(7/2,5/2)^\circ_3$	$6p\,(5/2,1/2)_2$	2506.2476	B
40121.2613	2.2	5.5	4.8	1.85	–1.96	$5d\,(7/2,5/2)^\circ_4$	$6p\,(5/2,1/2)_3$	2491.6923	C
40141.7704	0.6	0.6	1.8	2.96	–0.72	$5d\,(7/2,3/2)^\circ_3$	$6p\,(7/2,3/2)_4$	2490.4192	B
40562.4538	2.2	4.8	–2.4	1.57	–1.65	$5d\,(5/2,3/2)^\circ_2$	$6p\,(5/2,3/2)_2$	2464.5886	C
40964.1248	3.0	4.5	7.7	1.88	0.12	$6p\,(7/2,3/2)_4$	$7\mathrm{s}\,(7/2,1/2)^\circ_4$	2440.4205	C
40982.7546	1.9	2.3	2.8	2.21	–1.03	$5d\,(5/2,3/2)^\circ_2$	$6p\,(5/2,3/2)_3$	2439.3111	C
41000.2563	0.7	1.0	0.4	2.72	–1.07	$5d\,(7/2,3/2)^\circ_5$	$6p\,(7/2,3/2)_5$	2438.2697	B
41060.095	11	14	27	1.08	–0.14	$6p\,(5/2,3/2)_3$	$7\mathrm{s}\,(5/2,1/2)^\circ_2$	2434.7161	C
41081.8797	3.4	6.7	4.2	1.61	–0.14	$6p\,(7/2,3/2)_4$	$7\mathrm{s}\,(7/2,1/2)^\circ_3$	2433.4249	D
41153.7289	8.2	16	–3.6	1.23	–0.09	$6p\,(5/2,3/2)_3$	$7\mathrm{s}\,(5/2,1/2)^\circ_3$	2429.1761	D
41440.9978	1.5	2.4	0.7	2.18	–1.20	$5d\,(5/2,3/2)^\circ_4$	$6p\,(5/2,3/2)_4$	2412.3358	C
41467.8439	3.0	28	–35	1.10	–0.66	$6p\,(7/2,3/2)_3$	$7\mathrm{s}\,(7/2,1/2)^\circ_4$	2410.7740	D
41480.395	11	15	–9.1	1.23	0.01	$6p\,(5/2,3/2)_2$	$7\mathrm{s}\,(5/2,1/2)^\circ_2$	2410.0444	C
41574.0297	8.3	42	–6.5	0.53	–0.78	$6p\,(5/2,3/2)_2$	$7\mathrm{s}\,(5/2,1/2)^\circ_3$	2404.6160	D
41585.5988	3.4	3.7	1.0	1.87	0.11	$6p\,(7/2,3/2)_3$	$7\mathrm{s}\,(7/2,1/2)^\circ_3$	2403.9470	D
42053.2176	8.1	6.9	–2.4	1.60	0.29	$6p\,(5/2,3/2)_4$	$7\mathrm{s}\,(5/2,1/2)^\circ_3$	2377.2138	D
42181.3310	3.4	4.3	–3.9	1.81	0.05	$6p\,(7/2,3/2)_2$	$7\mathrm{s}\,(7/2,1/2)^\circ_3$	2369.9931	D
42191.5973[e]	2.0	1.5		2.49	–0.82	$5d\,(5/2,5/2)^\circ_0$	$6p\,(5/2,3/2)_1$	2369.4164	B
42226.4628	3.0	2.6	–1.9	2.13	0.37	$6p\,(7/2,3/2)_5$	$7\mathrm{s}\,(7/2,1/2)^\circ_4$	2367.4599	D
42258.2811	2.1	18	14	1.33	–2.25	$5d\,(7/2,5/2)^\circ_2$	$6p\,(5/2,1/2)_3$	2365.6771	C
42262.5943	0.6	1.0	–0.5	2.84	–0.83	$5d\,(7/2,3/2)^\circ_5$	$6p\,(7/2,3/2)_4$	2365.4357	B
42340.4865	1.6	2.0	2.5	2.24	–0.94	$5d\,(5/2,3/2)^\circ_4$	$6p\,(5/2,3/2)_3$	2361.0837	C
42386.2971	2.1	8.9	4.4	1.60	–1.99	$5d\,(7/2,3/2)^\circ_4$	$6p\,(5/2,1/2)_3$	2358.5317	C
42619.3889	1.8	12	–16	1.23	–2.40	$5d\,(7/2,5/2)^\circ_2$	$6p\,(5/2,1/2)_2$	2345.6315	D
42759.0451	1.4	1.2	–0.1	3.33	0.04	$6s\,(5/2,1/2)^\circ_2$	$6p\,(5/2,3/2)_1$	2337.9697	A
42844.914	11	16	–22	1.11	–0.11	$6p\,(5/2,3/2)_1$	$7\mathrm{s}\,(5/2,1/2)^\circ_2$	2333.2836	D
43186.6586	1.5	1.6	3.8	2.46	–1.28	$5d\,(7/2,5/2)^\circ_1$	$6p\,(5/2,1/2)_2$	2314.8183	C
43192.8155	0.5	0.4	0.2	3.99	0.27	$6s\,(7/2,1/2)^\circ_3$	$6p\,(7/2,3/2)_2$	2314.4883	A
43290.3009	0.8	0.7	0.2	3.78	0.44	$6s\,(5/2,1/2)^\circ_3$	$6p\,(5/2,3/2)_4$	2309.2758	A
43364.4095	0.4	0.3	–0.1	4.31	0.56	$6s\,(7/2,1/2)^\circ_4$	$6p\,(7/2,3/2)_5$	2305.3290	A
43405.1809	2.1				–1.98	$5d\,(7/2,3/2)^\circ_3$	$6p\,(5/2,1/2)_3$	2303.1634	G
43766.2887	1.8	17	–5.8	1.13	–2.52	$5d\,(7/2,3/2)^\circ_3$	$6p\,(5/2,1/2)_2$	2284.1587	C
43769.4888	1.8	3.0	–0.5	2.62	–0.65	$6s\,(5/2,1/2)^\circ_3$	$6p\,(5/2,3/2)_2$	2283.9917	B
43788.5477	0.4	0.4	–0.4	4.02	0.34	$6s\,(7/2,1/2)^\circ_3$	$6p\,(7/2,3/2)_3$	2282.9975	A
44123.0284	0.7	14	9.9	3.23	–0.49	$6s\,(7/2,1/2)^\circ_4$	$6p\,(7/2,3/2)_3$	2265.6893	E
44123.5635	1.8	5.3	6.2	3.45	0.20	$6s\,(5/2,1/2)^\circ_2$	$6p\,(5/2,3/2)_2$	2265.6618	E
44189.7896	1.3	1.4	–3.0	3.40	0.18	$6s\,(5/2,1/2)^\circ_3$	$6p\,(5/2,3/2)_3$	2262.2660	A
44292.2669	0.5	0.7	–1.3	3.73	0.06	$6s\,(7/2,1/2)^\circ_3$	$6p\,(7/2,3/2)_4$	2257.0314	A
44543.8643	1.6	2.2	1.7	3.21	0.00	$6s\,(5/2,1/2)^\circ_2$	$6p\,(5/2,3/2)_3$	2244.2818	A
44626.7475	0.5	0.5	–1.3	3.99	0.34	$6s\,(7/2,1/2)^\circ_4$	$6p\,(7/2,3/2)_4$	2240.1132	A
44797.6659	0.8	6.4	–11	1.73	–1.92	$5d\,(7/2,3/2)^\circ_2$	$6p\,(7/2,3/2)_2$	2231.5656	D
44875.1399	2.3	7.1	–9.2	1.69	–1.61	$5d\,(7/2,5/2)^\circ_5$	$6p\,(5/2,3/2)_4$	2227.7125	D
45393.3981	0.8	1.4	0.4	2.83	–0.88	$5d\,(7/2,3/2)^\circ_2$	$6p\,(7/2,3/2)_3$	2202.2761	B
45478.7464	2.0	4.3	–3.6	2.16	–1.18	$5d\,(7/2,5/2)^\circ_3$	$6p\,(5/2,3/2)_4$	2198.1428	C
45957.9343	2.1	27	–23	0.74	–2.51	$5d\,(7/2,5/2)^\circ_3$	$6p\,(5/2,3/2)_2$	2175.2211	D
46072.8455	2.2	39	–64	1.08	–2.30	$5d\,(7/2,5/2)^\circ_4$	$6p\,(5/2,3/2)_4$	2169.7952	D

Table 3. *Continued.*

σ_{Ritz} (cm^{-1})	u_{Ritz}	u_{obs} (10^{-3} cm^{-1})	$(\sigma_{Ritz} - \sigma_{obs})$	$\log I^a$	$\log gf^b$	Transition lower	Transition upper	λ^c (Å)	Source^d
46277.563^f	61	46		1.24		$6p\,(7/2,3/2)_4$	$6d\,(7/2,3/2)^\circ_3$	2160.1957	D
46378.2351	1.8	4.1	1.1	2.22	–1.00	$5d\,(7/2,5/2)^\circ_3$	$6p\,(5/2,3/2)_3$	2155.5061	C
46527.132	39	29		1.28		$6p\,(7/2,3/2)_4$	$6d\,(7/2,3/2)^\circ_4$	2148.6072	D
47173.140	12	13	–9.2	1.72		$6p\,(7/2,3/2)_4$	$6d\,(7/2,5/2)^\circ_4$	2119.1800	D
47207.815	22	25	–8.8	1.34		$6p\,(7/2,3/2)_3$	$6d\,(7/2,5/2)^\circ_2$	2117.6232	C
47302.324	30	36	–30	1.07		$6p\,(5/2,3/2)_3$	$6d\,(5/2,5/2)^\circ_3$	2113.3917	D
47373.811	32	24		1.04		$6p\,(5/2,3/2)_2$	$6d\,(5/2,5/2)^\circ_2$	2110.2023	D
47388.611^f	16	12	–1.0	1.99		$6p\,(7/2,3/2)_4$	$6d\,(7/2,5/2)^\circ_5$	2109.5431	D
47452.129	25	25	–9.8	1.45		$6p\,(5/2,3/2)_3$	$6d\,(5/2,5/2)^\circ_3$	2106.7190	C
47555.6774	2.0	29	–18	1.67	–1.90	$6s\,(7/2,1/2)^\circ_3$	$6p\,(5/2,1/2)_3$	2102.1313	D
47643.6940	8.3	23	37	1.00	–0.30	$6p\,(5/2,1/2)_2$	$7s\,(5/2,1/2)^\circ_3$	2098.2474	C
47676.859	12	13	9.1	1.84		$6p\,(7/2,3/2)_3$	$6d\,(7/2,5/2)^\circ_4$	2096.7876	D
47710.472^f	11	8.3		2.26		$6p\,(7/2,3/2)_5$	$6d\,(7/2,5/2)^\circ_6$	2095.3101	D
47722.625	30	29	19	1.40		$6p\,(5/2,3/2)_2$	$6d\,(5/2,5/2)^\circ_3$	2094.7765	C
47760.0500	3.0	34	–25	1.47	–0.27	$6p\,(7/2,1/2)_4$	$7s\,(7/2,1/2)^\circ_4$	2093.1348	D
47779.949	21	19	–2.2	1.81		$6p\,(7/2,3/2)_3$	$6d\,(7/2,5/2)^\circ_3$	2092.2630	D
47803.548	22	23	7.3	1.64		$6p\,(7/2,3/2)_2$	$6d\,(7/2,5/2)^\circ_2$	2091.2300	D
47877.8049	3.4	15	8.8	1.72	–0.02	$6p\,(7/2,1/2)_4$	$7s\,(7/2,1/2)^\circ_3$	2087.9862	D
47891.8045	1.8	22	–21	1.57	–1.64	$5d\,(7/2,5/2)^\circ_1$	$6p\,(5/2,3/2)_1$	2087.3757	D
47911.167	11	23	–6.2	1.23	0.03	$6p\,(5/2,1/2)_3$	$7s\,(5/2,1/2)^\circ_2$	2086.5320	C
47916.7852	1.7	34	–43	1.50	–2.21	$6s\,(7/2,1/2)^\circ_3$	$6p\,(5/2,1/2)_2$	2086.2874	D
48106.6692	3.0	23	–12	1.82	0.08	$6p\,(7/2,1/2)_3$	$7s\,(7/2,1/2)^\circ_4$	2078.0515	D
48375.681	21	29	4.9	1.45		$6p\,(7/2,3/2)_2$	$6d\,(7/2,5/2)^\circ_3$	2066.4941	D
48650.949^f	16	54	19	1.80		$6p\,(7/2,3/2)_5$	$6d\,(7/2,5/2)^\circ_5$	2054.8003	D
49256.3229	2.0	30	–55	1.85	–1.38	$5d\,(7/2,5/2)^\circ_1$	$6p\,(5/2,3/2)_2$	2029.5429	D
50029.4706	1.6	1.6	–2.0	3.63		$4f^{14}\,{}^1S_0$	$5d\,(5/2,5/2)^\circ_1$	1998.8218	C
53365.2255	2.6	11	–4.8	1.22		$4f^{14}\,{}^1S_0$	$5d\,(5/2,3/2)^\circ_1$	1873.8794	D

[a] Logarithm of calibrated intensity measured in source D, normalized so that the lowest value is 1.00. [b] Experimental $\log gf$ taken from Table 1. [c] Air wavelengths above 2000 Å, calculated with refractive index of air from [23], vacuum wavelengths below 2000 Å. [d] The discharge current and source σ_{Ritz} was measured at: 0.30 A (A), 0.60 A (B, F) 0.90 A (C) 1.02 A (D) in the PD and 0.44 A (E) in the HC. A–E were measured in the region 30 000 to 52 000 cm^{-1}, while F was measured in 22 000 to 44 000 cm^{-1}. [e] New line used to define the 45 421.045 cm^{-1} level. [f] New transition suggested in [3].

5.3 Further analysis of the Penning discharge

For the measured lifetimes to be accurate, it must be shown that the collisional rate between the excited levels and other particles in the discharge plasma is significantly lower than the inverse of the lifetimes; otherwise, the values will be underestimated. It is shown in Figure 4 that lifetime measurement of the 39 721 cm^{-1} level is affected by collisional deexcitation. In the absence of self-absorption and an assumed radiative lifetime of 260 ns for this level, the apparent lifetimes obtained for the currents 0.1 and 0.4 A at 0.118 torr give collisional frequencies of 0.70 and 4.5 MHz, respectively. This is far too low to have any significant influence on the lifetimes of the $6p$ levels, being about two orders of magnitude smaller than the lifetime of the 39 721 cm^{-1} level. There is, however, a factor that can render this conclusion invalid. The collisional cross section of the $6p$ levels, which are unknown, can be much larger than that of the 39 721 cm^{-1} level. With collisional frequencies in the MHz-range and a pulse rate of 10 Hz for the pump laser, it is safe to assume that the PD-plasma reaches equilibrium between each lifetime measurement, i.e. the population of the lower pump level is restored. Note that the laser pulses are shorter than 1 ns, which means that the collisional frequencies are too low to change the population of the lower pump level during the pulse.

In an ordinary Boltzmann plot $\ln(I_k/g_kA_k)$ is plotted versus the energy, E, of the upper level [17]. Here, I_k is the line intensity, which is proportional to the number of photons, g_k the statistical weight of the upper level and A_k the transition probability. A set of transitions from different levels produces a straight line with the slope $-1/kT$ if the plasma under investigation is in thermal equilibrium, i.e. the population distribution is determined by collisions. In a Boltzmann plot of observed Yb III transitions the datapoints deviate, however, systematically from a straight line, see Figure 8. From the lifetimes presented in Table 1 it is evident that the $6p$ levels are divided into two groups depending on the lifetimes, one about 1.5 ns and the another about 2.2 ns. Each group gives a straight line of the same slope in the Boltzmann plot. There is, however, a shift in $\ln(I_k/g_kA_k)$ of 0.4 between the groups, which is the same as the natural logarithm of the ratio between

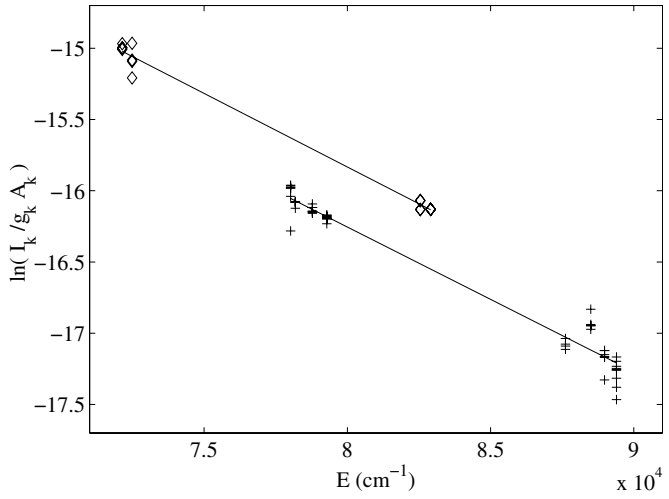

Fig. 8. Ordinary Boltzmann plot for observed Yb III transitions in a PD-spectrum, which were recorded at a discharge current of 0.60 A and a neon pressure of 0.013 torr. The data points are divided into two sets depending on the approximate lifetime of the upper level: diamonds 2.2 ns and crosses 1.5 ns. The upper line corresponds to an excitation temperature of 13 900 K and the lower of 14200 K. Uncertainties have not been considered when fitting the data. Weak transitions have, however, not been included in the plot.

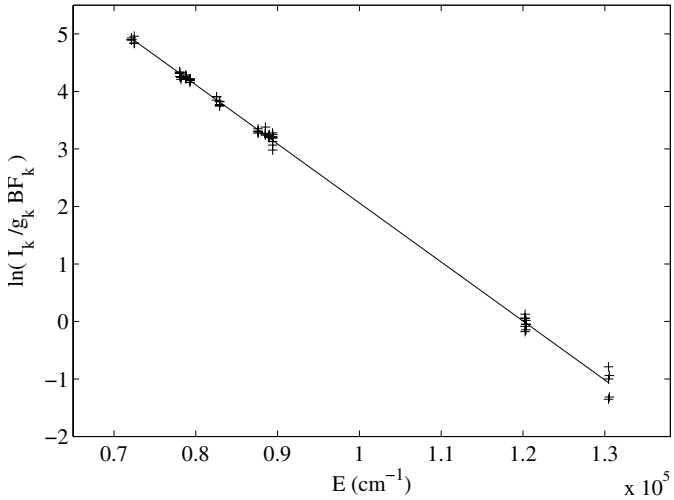

Fig. 9. Modified Boltzmann plot for the same Yb III transitions as in Figure 8. The data have also been extended towards higher level energies. The fitted line corresponds to a excitation temperature of 14 300 K. Error bars have not been depicted, but the fitted line falls within two standard deviations of all data points.

the approximate lifetimes of the two groups. Therefore, if A_k is replaced with BF_k in the Boltzmann plot, i.e. $\ln(I_k/g_k BF_k)$ is plotted versus E, the two groups define the same line, see Figure 9.

A probable explanation to the linear behavior in Figure 9 is that there is a Boltzmann distribution of the level population. This is a result of a narrow spread of the collisional cross-sections of the $6p$, $6d$ and $7s$ levels and of Maxwell distributed electron velocities. The collisional rate is, however, too low to depopulate the energy levels. Instead, deexcitation occurs through spontaneous emission, i.e. the levels are in coronal equilibrium, which explains why there is no dependence on the lifetimes. If the scenario presented here is true, the measured lifetimes of the $6p$ levels are not affected by collisional deexcitation. Further, the electron temperature can be determined from the slope $-1/kT$ of the fitted line in Figure 9.

When determining the electron temperatures from different spectra using the proposed method, all fell somewhere between 14 000 and 14 300 K for currents between 0.30 and 1.02 A. Clearly, the thermalization of the sputtered electrons is insensitive to changes in the current, which can be explained by a combination of three factors. Firstly, the population distribution of the Yb III levels is independent of the collisional rate, i.e. the electron density, which is strongly coupled with the current. Secondly, the energy of thermalized electrons and also of secondary electrons formed when the gas is ionized is dependent on the energy of the sputtered electrons, which is strongly coupled to the voltage over the PD-source. The voltage, however, changes only slowly with the current, see Section 4.3. Thirdly, the number density of neon in the plasma is much higher than of ionized ytterbium, which means that the probability is high for an electron to be thermalized before it collides with an ytterbium ion. Unfortunately, it is not possible to investigate any pressure dependence for the excitation temperature, since all spectra were recorded at neon pressures within a narrow interval.

The resonance lines of Mg I and Mg II are present in the PD-spectra, since the aluminum of the cathode insets contains magnesium to a fraction of a percent. From the Doppler width of the Mg II resonance transition at 35 761 cm^{-1}, which could be fitted with a pure Gaussian function, the ion temperature was determined to be 2600 and 3970 K at the currents 0.30 and 0.90 A, respectively. These temperatures are overestimated, since the mass number of 24 of the lightest and most abundant isotope was used in the derivation. Further, Zeeman splitting, isotope shifts and hfs of the odd isotope, which broadens the line profile, have not been taken into account. However, the combined effect of the latter two on the width of the profile should be small [24]. This is further strengthened by the fact that there was no trace of any asymmetry of the line profiles in the residuals of the fit. In contrast, the least asymmetric $5d$–$6p$ transitions in Yb III give much larger residuals when fitted with a Gaussian function, which is a result of the isotope composition of ytterbium, see Section 4.3. This may explain the much larger apparent ion temperatures of Yb III. As an example, the 40 142 cm^{-1} transition gives temperatures of 8340 and 9670 K at a discharge current of 0.30 and 0.90 A, respectively, if a mass number of 173 is used.

The ratio between the temperatures measured for the Yb III transition is smaller than the ratio for the Mg II transition, indicating that the isotope components of the former have a much larger impact on the line profile. The mass number of magnesium is much smaller than for

ytterbium. Therefore, the large difference in temperature between Mg II and Yb III can also be explained by a faster thermalization of the sputtered magnesium through collisions with the neon buffer gas. Another unknown parameter is the initial energy of the sputtered atoms, which may be lower for magnesium than for ytterbium. It has been shown [6] that the ion temperature in a PD-source increases with lowered pressure. This could, however, not be confirmed due to the constant neon pressures of the FTS recordings.

6 Comparison with laser-ablation plasmas

From the results presented in Section 3.3 it is probable that the lifetime of the 39 721 cm^{-1} level measured in [10] is underestimated. It is stated in [10] that the error due to flight-out-of-view effects was insignificant, since the slit of the monochromator was oriented parallel to the path of the ablation-laser and that the delay time between the ablation pulse and the data sampling was set to probe Yb III ions with a velocity of 5 km/s. The velocity component perpendicular to the path of the ablation laser is smaller than the parallel component, but of the same order of magnitude [25,26]. It is not evident how this influenced the measured lifetimes in [10], but it probably resulted in underestimated values.

With the ion temperatures of Mg II at 0.30 A the rms velocity in one direction of the Yb III ions has an upper limit of 350 m/s. Note that the lifetimes around 260 ns for the 39 721 cm^{-1} level were measured at a discharge current of 0.10 A and pressures close to that of the FTS investigation. The fluorescence region of the plasma, a cylinder more than 1 mm in diameter, was imaged onto the monochromator slit, which had a width of 0.6 mm and was oriented parallel to the path of the pump laser. If a rms velocity of 350 m/s perpendicular to the orientation of the slit is assumed, 68% of the Yb III ions will cross the width of the slit in 1.7 μs, which is 6.6 times longer than the lifetime. This means that the flight-out-of-view effect introduces only a small error, which is further reduced by the fact that laser-excited ions also fly into the region where the slit is imaged in the plasma. Clearly, an advantage with a PD-plasma over a laser-ablation plasma is that the ion velocities are much lower, which enables the measurement of longer lifetimes. On the other hand, as was shown in Section 3.3, the measurements of the longer lifetimes in a PD-plasma are influenced by collisional deexcitation. This is also the case for laser-ablation plasmas, but due to the better control over the plasma parameters, it is easier to determine the size of the effect in a PD-source.

In a laser-ablation plasma line emission is present due to collisional excitation and recombination processes, which results in a time-dependent signal on top of the fluorescence signal that can sometimes influence the derived lifetimes [8]. Due to instabilities in the fluency of the laser, this background signal can also vary between different ablation pulses, making it hard to compensate for. The continuous discharge of the PD-source produces an even stronger background signal, which is constant in time and has, therefore, no direct influence on the measured lifetimes. The strength of this background is wavelength dependent and follows the distribution of the line intensity of the spectrum, which can result in a great increase of the noise in a fluorescence signal, especially if the channel is close to another strong transition. The size of this effect can, however, be reduced by using a monochromator with a narrow bandwidth.

The lifetimes of the $6p$ levels derived in this work has been measured by pumping from metastable levels between 34 656 and 51 582 cm^{-1} in a PD-plasma. In earlier works, where this method has been used on doubly-ionized elements in laser-produced plasmas, the lower pump levels have never been this high up in the level system. In order to get a high population density of the metastable levels in a laser-produced plasma, the delay between the pump and ablation pulses must be short and the pump pulse must interact with the plasma close to the ablation target. This will, however, also give a strong time-dependent background from the laser-produced plasma [2].

7 Conclusions

It has been shown that the plasma of a PD-source is suitable for measuring lifetimes in the nanosecond range by time-resolved LIF. In order to estimate the probability of success with the lifetime measurements, PD-spectra recorded under different discharge conditions were first studied. A number of strong spectral lines with lower metastable $5d$ and $6s$ levels were found. From the nature of these levels, it should be possible to momentarily increase the intensity of the lines drastically by pumping corresponding transitions with a pulsed laser, thereby, enabling lifetime measurements of the upper levels. This turned out to be the case. An initial study like this is recommended if the PD-source is to be used for lifetime measurements of other elements. If a transition is not prominent in the PD-spectrum, or if it has a lower level with a short lifetime, it can probably not be used for lifetime studies. Further, by studying spectra the optimal discharge conditions can also be found. Remember that either a sparse line spectrum or a narrow spectral bandwidth of the detection system is required for a high S/N of the fluorescence signal.

A lower limit to the lifetime of the 39 721 cm^{-1} level has been estimated to be about 250 ns. The influence of the discharge parameters on this lifetime was investigated and clear dependence on both the current and the pressure was found. A regression, including both these parameters, was attempted in order to derive the true radiative lifetime. Even though non-integer exponents of the parameters were tried, no satisfactory fit was found. It is possible that the regression would have been successful if the radiative lifetime were shorter, i.e. if the apparent lifetime were less sensitive to changes in the discharge parameters.

Lifetimes of nine $6p$ levels in Yb III have been measured. The remaining three $6p$ levels could not be investigated, since all strong downward transitions from these levels fell outside the wavelength coverage of the pump

laser. For the 6p levels, almost complete sets of branching fractions have been derived from FTS spectra of the PD-source. The transition probabilities presented in this work are in good agreement with the semi-empirical values in [3], from which an upper estimate of the relative error of the measured lifetimes have been derived. From the observed wavenumbers, the accuracy of the Yb III level energies, both absolute and relative, have been improved by about an order of magnitude.

The covariance matrix and energy levels from the fitting of the observed transitions to the level systems of Yb III are published as *Supplementary Online Material*. This enables the reader to calculate Ritz wavenumbers and uncertainties for transitions not included in Table 3.

One of the authors (KJÖ) would like to thank Dr. Hampus Nilsson for assisting the FTS measurements, Dr. Sven Huldt for rewarding discussions and Prof. Sveneric Johansson for support in writing the paper.

References

1. E.A. Den Hartog, J.E. Lawler, C. Sneden, Phys. Scripta **T119**, 45 (2005)
2. C.M. Sikström, M. Schultz-Johanning, M. Kock, Z.S. Li, H. Nilsson, S. Johansson, H. Lundberg, A.J.J. Raassen, J. Phys. B **32**, 5687 (1999)
3. E. Biémont, H.P. Garnir, Z.S. Li, V. Lokhnygin, P. Palmeri, P. Quinet, S. Svanberg, J.F. Wyart, Z.G. Zhang, J. Phys. B **34**, 1869 (2001)
4. W.C. Martin, R. Zalubas, L. Hagan, *Atomic Energy Levels - The Rare-Earth Elements* (NSRDS-NBS, National Bureau of Standards, U.S. Department of Commerce, Washington, 1978)
5. C. Heise, R. Kling, M. Kock, J. Hollandt, M. Kühne, Appl. Opt. **33**, 5111 (1994)
6. R. Kling, *Entwicklung und Untersuchung einer Penningentladung zur Erzeugung von XUV Strahlung und als spektroskopische Lichtquelle höher ionisierter Spezies (thesis)* (Herbert Utz Verlag Wissenschaft, München, 1997)
7. Z.S. Li, J. Norin, A. Persson, C.G. Wahlström, S. Svanberg, P.S. Doidge, E. Biémont, Phys. Rev. A **60**, 198 (1999)
8. Z.S. Li, H. Lundberg, G.M. Wahlgren, C.M. Sikström, Phys. Rev. A **62**, 032505 (2000)
9. A. Persson, *Programpaket för utvärdering och presentation av fysikaliska mätdata* (Lund Reports on Atomic Physics 259, Lund, 1993)
10. Z.G. Zhang, Z.S. Li, S. Svanberg, P. Palmeri, P. Quinet, E. Biémont, Eur. Phys. J. D **15**, 301 (2001)
11. A.P. Thorne, C.J. Harris, I. Wynne-Jones, R.C.M. Learner, G. Cox, J. Phys. E **20**, 54 (1987)
12. K.J. Öberg, Eur. Phys. J. D **41**, 25 (2007)
13. D.S.G. Pollock, *A handbook of time-series analysis, signal processing and dynamics* (Academic Press, San Diego, 1999)
14. K.J.R. Rosman, P.D.P. Taylor, Pure Appl. Chem. **70**, 217 (1998)
15. C.M. Sikström, H. Nilsson, U. Litzén, A. Blom, H. Lundberg, J. Quant. Spectrosc. Radiat. Transfer **74**, 355 (2002)
16. J. Hollandt, U. Becker, W. Paustian, M. Richter, G. Ulm, Metrologia **37**, 563 (2000)
17. A. Thorne, U. Litzén, S. Johansson, *Spectrophysics* (Springer-Verlag, Berlin, Heidelberg, 1999)
18. B.W. Bryant, J. Opt. Soc. Am. **55**, 771 (1965)
19. B.W. Bryant, John Hopkins Spectr. Report No. 21, Ph.D. thesis (1961)
20. J. Sugar, J. Opt. Soc. Am. **60**, 571 (1970)
21. W.F. Meggers, C.H. Corliss, J. Res. Nat. Bur. Stand. **70** (1966)
22. V. Kaufman, J. Sugar, J. Opt. Soc. Am. **66**, 1019 (1976)
23. B. Edlén, Metrologia **2**, 71 (1966)
24. J.C. Pickering, A.P. Thorne, J.K. Webb, Mon. Not. R. Astron. Soc. **300**, 131 (1998)
25. A. Mele, A. Giardini Guidoni, C. Flamini, R. Kelly, A. Miotello, S. Orlando, R. Teghil, Nucl. Instr. Meth. Phys. Res. B **116**, 257 (1996)
26. K. Sasaki, S. Matsui, H. Ito, K. Kadota, J. Appl. Phys. **92**, 6471 (2002)